Struct Multidisc Optim (2009) 38:469–489
DOI 10.1007/s00158-008-0300-1

RESEARCH PAPER

Optimal design of periodic functionally graded composites with prescribed properties

Glaucio H. Paulino · Emílio Carlos Nelli Silva · Chau H. Le

Received: 6 July 2007 / Revised: 10 May 2008 / Accepted: 5 July 2008 / Published online: 23 September 2008

Abstract The computational design of a composite where the properties of its constituents change gradually within a unit cell can be successfully achieved by means of a material design method that combines topology optimization with homogenization. This is an iterative numerical method, which leads to changes in the composite material unit cell until desired properties (or performance) are obtained. Such method has been applied to several types of materials in the last few years. In this work, the objective is to extend the material design method to obtain functionally graded material architectures, i.e. materials that are graded at the local level (e.g. microstructural level). Consistent with this goal, a continuum distribution of the design variable inside the finite element domain is considered to represent a fully continuous material variation during the design process. Thus the topology optimization naturally leads to a smoothly graded material system. To illustrate the theoretical and numerical approaches, numerical examples are provided. The homogenization method is verified by considering one-dimensional material gradation profiles for which analytical solutions for the effective elastic properties are available. The verification of the homogenization method is extended to two dimensions considering a trigonometric material gradation, and a material variation with discontinuous derivatives. These are also used as benchmark examples to verify the optimization method for functionally graded material cell design. Finally the influence of material gradation on extreme materials is investigated, which includes materials with near-zero shear modulus, and materials with negative Poisson's ratio.

Keywords Material design · Functionally graded materials · Optimization · Homogenization · Extreme materials · Zero shear-modulus materials · Negative Poisson's ratio materials

G. H. Paulino · C. H. Le
Department of Civil and Environmental Engineering,
University of Illinois at Urbana-Champaign,
Newmark Laboratory, 205 North Mathews Avenue,
Urbana, IL 61801, USA

E. C. N. Silva (✉)
Department of Mechatronics and Mechanical Systems,
Escola Politécnica da Universidade de São Paulo,
Av. Professor Mello Moraes, 2231,
São Paulo, São Paulo 05508-900, Brazil
e-mail: ecnsilva@usp.br

Nomenclature

List of Symbols:

A	assembling operator
$\mathbf{D}$	elasticity tensor
D_{ijkl}	index notation for elasticity tensor
D^*_{ijkl}	index notation for desired tensor properties
$\mathbf{D}^H$	homogenized tensor properties
D^H_{rspq}	index notation for homogenized tensor properties
D^H_{ij}	matrix notation for homogenized tensor properties
$\mathbf{D}^m$	elasticity tensor of the mixture
d_n	design variables associated with nodes
E^m	Young's modulus of mixture
E^+, E^-	Young's modulus of materials + and −

e	element e
f	projection function
$\mathbf{F}^{(mn)}$	nodal force vector for load case mn
$F_{iI}^{e(mn)}$	component of nodal force vector for load case mn
$\mathbf{F}^{e(mn)}$	finite element nodal force vector for load case mn
G	shear modulus
$G_{\max}$, $G_{\min}$	upper and lower limits of shear modulus
G^m	shear modulus of the mixture
G^+, G^-	shear modulus of materials + and −
H_{per}	set of Y-periodic functions
i, j, k, l	indices
$\mathbf{I}$	identity tensor
I	index
$\mathbf{K}$	stiffness matrix
$\mathbf{K}^e$	finite element stiffness matrix
$K^e_{(iIjJ)}$	term of finite element stiffness matrix
K	bulk modulus
$K_{\max}$, $K_{\min}$	upper and lower limits of bulk modulus
K^m	bulk modulus of the mixture
K^+, K^-	bulk modulus of materials + and −
m_I	elements associated with I-th node
mn	load case number
N_I	finite element shape function
N	number of finite elements
n_d	number of nodes per finite element
NDV	number of design variables
$NEXCL$	number of elements explicitly excluded from the optimization
r_{min}	radius of circle
r_{ij}	distance between nodes j and i
R^3	3D space of real numbers
S_i	set of nodes in the domain of influence of node i
$\mathbf{u}^\epsilon$	displacement inside the unit cell
$\mathbf{u}_0$	zero order term of displacement
$\mathbf{u}_1$	first-order variation of displacement
$\mathbf{v}$	displacement vector
V_i	relative volume of each finite element
v_i	component of vector $\mathbf{v}$
$\mathbf{x}$	coordinates associated with the composite macro-dimensions
$\mathbf{x}_j$	position vector of node j
x, y	cartesian coordinates
$\mathbf{y}$	coordinates associated with the composite micro-dimensions
$\mathbf{Y}$	unit cell domain
Y	unit cell volume
Y_i	maximum value of coordinate i of unit cell domain
W	objective function
w_{ijkl}	weight coefficient
w	weight function
∂	differential operator
$\boldsymbol{\partial}_x$	differential operator for macro coordinates
$(\partial_x)_{ij}(.)$	index notation for differential operator for macro coordinates
$\boldsymbol{\partial}_y$	differential operator for micro coordinates
$\left(\partial_y\right)_{ij}(.)$	index notation for differential operator for micro coordinates
$\boldsymbol{\chi}$	characteristic displacement function of the unit cell
$\chi_i^{(mn)}$	component of characteristic displacement function for load case mn
$\widehat{\boldsymbol{\chi}}^{(mn)}$	nodal values of the characteristic function $\boldsymbol{\chi}$ for load case mn
δ	variational operator
δ_{im}	kronecker delta
$\boldsymbol{\varepsilon}$	strain
$\boldsymbol{\varepsilon}^\epsilon$	strain inside unit cell
ε_{kl}	index notation for strain
ϵ	parameter
Φ	function of interest
κ	interpolation factor
υ^m	Poisson's ratio of mixture
υ^+, υ^-	Poisson's ratio of materials + and −
Θ	averaged volume fraction
ρ	pseudo-density distribution function (design variable)
ρ_I	nodal pseudo-density function (design variable)
ρ_{low}	lower bound for design variables ρ_I
σ_{ij}	index notation for stress
Ω	domain volume
Ω^e	finite element volume
$\cup$	union operator

1 Introduction

Functionally Graded Materials (FGMs) possess continuously graded properties and are characterized by spatially varying microstructures created by nonuniform distributions of the reinforcement phase as well as by interchanging the role of reinforcement and matrix (base) materials in a continuous manner. The smooth variation of properties may offer advantages such as local reduction of stress concentration and increased bonding strength (see, for example, Miyamoto et al. 1999; Suresh and Mortensen 1988; Paulino et al. 2003).

Standard composites result from the combination of two or more materials, usually resulting in materials that offer advantages over conventional materials. The unit cell is the smallest structure that is periodic in the composite matrix. By changing the volume fraction of the constituents, the shape of the inclusions, or even the topology of the unit cell, we can obtain different effective properties for the composite material (Torquato 2002). Therefore, when designing composites, we can tailor the properties to a specific application (which, in general, cannot be done with a single material). At the macroscale observation, traditional composites (e.g. laminated) exhibit a sharp interface among the constituent phases which may cause problems such as stress concentration, and scattering (if a wave is propagating inside the material), among others. However, a material made using the FGM concept would maintain some of the advantages of traditional composites and alleviate problems related to the presence of sharp interfaces at the macroscale. The design of the composite material itself is a difficult task, and the design of a composite where the properties of its constituent materials change gradually in the unit cell domain is even more complex. Meanwhile, this design can be successfully achieved by using a *material design method*, as described below.

The overall objective of material design is to generate composite materials with prescribed or improved properties not found in common materials. This can be achieved by modifying the microstructure of the composite material (Torquato 2002). In traditional composite designs, such as fiber- or sphere-reinforced and laminated materials, the change in the properties is obtained by modifying the location, orientation, material constituents, or volume fraction of the fiber, sphere, or laminar inclusion, respectively (Cherkaev and Kohn 1997). This allows some control of the composite properties. A more systematic approach to design composite materials has been developed in recent years, which combines topology optimization with homogenization to change the composite material unit cell topology until desired properties or performance are obtained. The approach consists of finding the distribution of different material phases in a periodic unit cell that optimizes the properties or performance characteristics of the resulting composite system (Cherkaev and Kohn 1997; Cherkaev 2000).

In the process of designing materials with prescribed and improved properties, a natural question related to the achievable properties in the material design process arises. Based on the fact that the constitutive elasticity matrix must be positive definite for elastic materials, Milton and Cherkaev (1995) have shown the existence of materials for thermodynamically admissible sets by layering and combining an infinitely rigid material with voids (infinite compliance). However, the extreme condition of this admissible set, such as isotropic material with Poisson's ratio equal to -1 ($\nu = -1$), cannot be reached in practice because an infinitely rigid material does not exist.

Other bounds were derived in the past. Considering materials with finite properties, we can cite, for example, the work of Hashin and Shtrikman (1963) for bounds of an isotropic mixture of classical materials using energy analyses, the work of Lipton and Northrup (1994) (among others) that defined the bounds for orthotropic mixtures of isotropic materials, and the work of Cherkaev and Gibiansky (1993) that improved the classical Hashin and Shtrikman (1963) estimates of the effective properties for an isotropic mixture assembled from two isotropic elastic materials. Bounds for elasticity and conductivity properties of mixtures of two materials (not necessarily isotropic) were developed by Gibiansky and Torquato (1995) and Cherkaev and Gibiansky (1996). Attainable properties for piezoelectric materials were discussed by Smith (1992) considering the positive definiteness of a tensor involving elastic, piezoelectric, and dielectric properties, however, no bounds were obtained. Gibiansky and Torquato (1999) also discussed optimal bounds for piezoelectric matrix laminate composites. However, the extremal properties that can be achievable by composite designs is limited, and has been explored mainly for elasticity and conductivity (Sigmund 2000; Cherkaev and Gibiansky 1993; Gibiansky and Sigmund 2000; Larsen et al. 1997).

In the past few years, the material design concept based on topology optimization and homogenization has been applied to design elastic (Sigmund 1994, 1995; Neves et al. 2002; Diaz and Benard 2003; Guedes et al. 2003; Neves et al. 2000), thermoelastic (Sigmund and Torquato 1996, 1997; Chen et al. 2001; Torquato et al. 2003), piezoelectric (Silva et al. 1998, 1999a, b; Sigmund et al. 1998; Sigmund and Torquato 1999), phononic (Sigmund and Jensen 2003), and photonic (Cox and Dobson 1999, 2000) composite materials, among others. In addition, manufacturing techniques have also been studied to build such materials (Qi and Halloran 2004; Van Hoy et al. 1998; Crumm and Halloran 1998; Qi et al. 2004; Mazumder et al. 1999, 2000; Crumm et al. 2007). However, processing techniques have not been explored when material gradation is considered inside the unit cell, and have concentrated in the traditional (1–0) design (Qi et al. 2004; Mazumder et al. 2000). This paper explores the computational design of periodic

functionally graded microstructures. The manufacturing of such materials is beyond the scope of the present work and is a subject of future research.

This paper is organized as follows. In Section 2, a brief introduction about topology optimization for FGM structures is given. In Section 3, the theoretical formulation of homogenization for FGM composite materials is addressed. In Section 4, the formulation of the composite material design problem based on continuous topology optimization is presented, and in Section 5 the material model applied is described. The numerical implementation, including an applied gradient control for material gradation, is discussed in Section 6. The sensitivity analysis is briefly described in Section 7. In Section 8, some representative results are presented to illustrate homogenization and material design concepts. The influence of FGM gradation in the design of extreme materials such as minimum shear stiffness and negative Poisson's ratio materials is discussed. Finally, in Section 9, concluding remarks are provided.

2 Topology optimization

A major concept in topology optimization is the extended design domain, which is a large fixed domain that must contain the whole structure to be determined by the optimization procedure. The objective is to determine the holes and connectivities of the structure by adding and removing material in this domain. Because the extended domain is fixed, the finite element model is not changed during the optimization process, which simplifies the calculation of derivatives of functions defined over the extended domain (Bendsøe and Kikuchi 1988; Allaire 2002). *In the case of material design, the extended design domain is the unit cell domain.*

The discrete problem, where the amount of material at each element can assume only values equal to either one or zero (i.e. void or solid material, respectively), is an ill-posed problem. A typical way to seek a solution for topology optimization problems is to relax the problem by allowing the material to assume intermediate property values during the optimization procedure, which can be achieved by defining a special material model (Cherkaev 2000; Allaire 2002; Kohn and Strang 1986a, b, c; Murat and Tartar 1985). Essentially, the material model approximates the material distribution by defining a function of a continuous parameter (design variable) that determines the mixture of basic materials throughout the domain. In this sense, the relaxation yields a continuous material design problem that no longer involves a discernible connectivity. A topology solution can be obtained by applying penalization coefficients to the material model to recover the 0–1 design (and thus, a discernible connectivity), and some gradient control on material distribution, such as a filter or projection (Bendsøe and Sigmund 2003).

It turns out that this relaxed problem is strongly related to the FGM design problem, which essentially seeks a continuous transition of material properties (Paulino and Silva 2005; Silva and Paulino 2004). Thus, while the 0–1 design problem (needs complexity control, such as filter) does not admit intermediate values of design variables, the FGM design problem admit solutions with intermediate values of the material field.

Early work on material design followed a traditional topology optimization formulation, where the design variables are defined in a piecewise fashion in the discretized domain, which means that continuity of the material distribution is not realized between finite elements. However, considering that the topology optimization results in a smoothly graded material, a more natural way of representing the material distribution emerges by considering a continuous representation of material properties (Matsui and Terada 2004; Rahmatalla and Swan 2004), which is achieved by interpolating the properties inside the finite element using shape functions (Matsui and Terada 2004; Rahmatalla and Swan 2003; Guest et al. 2004). The concept of employing continuum interpolation of material distribution inside the finite element has been implemented to model FGMs, originating the so-called "graded finite element" (Kim and Paulino 2002) . Thus, nodal design variables are defined rather than the usual element based design variables.

The objective of the present work is to design FGM composites using the concept of the relaxed problem in continuum topology optimization. Thus, the design of elastic FGM composites to achieve desired properties is addressed. The problem is posed by minimizing the square difference between homogenized and desired properties. A continuum distribution of the design variable inside the finite element domain is considered allowing representation of a continuous material variation during the design process. Since we are interested in solutions with a continuous distribution of material, we allow for intermediate materials (no penalization). A material model based on the Hashin and Shtrikman bounds is employed to guarantee that the final composite can be achieved by a mixture of basic materials used in the design. A gradient control constraint in the unit cell domain is implemented based on projection techniques (Guest et al. 2004; Carbonari et al. 2007). This gradient control capability permits to address the influence of FGM gradation in the design of extreme materials. It also avoids the problem of

mesh dependency in the topology optimization implementation (Bendsøe and Sigmund 2003). The actual optimization problem is solved by the MMA ("Method of Moving Assymptotes") algorithm (Svanberg 1987; Bruyneel et al. 2002).

3 Homogenization method

Homogenization allows the calculation of the effective properties of a complex periodic composite material from its unit cell topology. It is a general method for calculating effective properties and has no limitations regarding volume fraction or shape of the composite constituents. The main assumptions are that the unit cell is periodic and that the scale of the composite part is much larger than the microstructure dimensions (Cherkaev and Kohn 1997; Allaire 2002; Guedes and Kikuchi 1990).

This section addresses details of the theoretical and computational aspects of the homogenization method applied to FGM composites. Considering the standard homogenization procedure for elastic materials, the unit cell is defined as $\mathbf{Y} = [0, Y_1] \times [0, Y_2] \times [0, Y_3]$ and the elastic property function D_{ijkl} is considered to be a $\mathbf{Y}$-periodic function:

$$\mathbf{D}^{\epsilon}(\mathbf{x}) = \mathbf{D}(\mathbf{x}, \mathbf{y}); \quad \mathbf{D}(\mathbf{x}, \mathbf{y}) = \mathbf{D}(\mathbf{x}, \mathbf{y}+Y)$$
$$\text{and } \mathbf{y} = \mathbf{x}/\epsilon\,, \epsilon > 0, \tag{1}$$

where ϵ is a parameter of small magnitude representing the microscale in which the properties are changing (composite microstructure scale), $\mathbf{x}$ and $\mathbf{y}$ are the coordinates associated with the composite macro- and micro-dimensions, respectively (see Fig. 1). Expanding the displacement $\mathbf{u}$ inside the unit cell, we get (Allaire 2002; Sanchez-Palencia 1980):

$$\mathbf{u}^{\epsilon} = \mathbf{u}_0(\mathbf{x}) + \epsilon \mathbf{u}_1(\mathbf{x}, \mathbf{y}), \tag{2}$$

where only the first-order variation terms ($\mathbf{u}_1(\mathbf{x}, \mathbf{y})$) are taken into account because dispersive behavior is not considered, and $\mathbf{u}_1$ is Y-periodic. The strain is written as (Allaire 2002; Guedes and Kikuchi 1990; Sanchez-Palencia 1980):

$$\boldsymbol{\varepsilon}^{\epsilon} = \boldsymbol{\partial}_x \mathbf{u}^{\epsilon} = \boldsymbol{\partial}_x \mathbf{u}_0(\mathbf{x}) + \epsilon \boldsymbol{\partial}_x \mathbf{u}_1(\mathbf{x}, \mathbf{y}) + \boldsymbol{\partial}_y \mathbf{u}_1(\mathbf{x}, \mathbf{y}), \tag{3}$$

where $\boldsymbol{\varepsilon}$ is the mechanical strain and, by definition

$$(\partial_x)_{ij}(.) = \frac{1}{2}\left(\frac{\partial(.)_i}{\partial x_j} + \frac{\partial(.)_j}{\partial x_i}\right)$$
$$(\partial_y)_{ij}(.) = \frac{1}{2}\left(\frac{\partial(.)_i}{\partial y_j} + \frac{\partial(.)_j}{\partial y_i}\right). \tag{4}$$

Equations (2) and (3), together with properties (1), must be substituted into the energy functional for the elastic medium, and the variation of this functional taken in relation to $\mathbf{u}^{\epsilon}$. Considering the limit $\epsilon \to 0$, we have that (Allaire 2002; Sanchez-Palencia 1980),

$$\lim_{\epsilon \to 0} \int_{\Omega} \Phi\left(\mathbf{x}, \frac{\mathbf{x}}{\epsilon}\right) d\Omega = \frac{1}{|Y|} \int_{\Omega} \int_{Y} \Phi\left(\mathbf{x}, \frac{\mathbf{x}}{\epsilon}\right) dY\, d\Omega, \tag{5}$$

where Φ denotes the function of interest. By means of the terms related to $\delta\mathbf{u}_1(\mathbf{x}, \mathbf{y})$ and $\delta\mathbf{u}_0(\mathbf{x})$, we obtain the microscopic and macroscopic equations, respectively. Due to the linearity of the problem, and assuming the separation of variables for $\mathbf{u}_1(\mathbf{x}, \mathbf{y})$, we obtain:

$$\mathbf{u}_1 = \boldsymbol{\chi}(\mathbf{x}, \mathbf{y})\, \boldsymbol{\varepsilon}(\mathbf{u}_0(\mathbf{x})) \quad \text{and}$$
$$\boldsymbol{\partial}_y \mathbf{u}_1(\mathbf{x}, \mathbf{y}) = \boldsymbol{\partial}_y \boldsymbol{\chi}(\mathbf{x}, \mathbf{y})\, \boldsymbol{\partial}_x(\mathbf{u}_0(\mathbf{x})), \tag{6}$$

where $\boldsymbol{\chi}(\mathbf{x}, \mathbf{y})$ are the characteristic displacements of the unit cell due to each possible initial strain, which is also Y-periodic, belonging to $H_{per}(Y, R^3)$:

$$H_{per}(Y, R^3) = \left\{\mathbf{v} = (v_i)\,|v_i \in H_{per}(Y), i = 1, 2, 3\right\}$$
$$H_{per}(Y) = \left\{v \in H^1(Y)\,\middle|\, v \text{ takes equal values on opposite sides of } Y\right\}, \tag{7}$$

which corresponds to the periodicity condition in the unit cell (see Fig. 2).

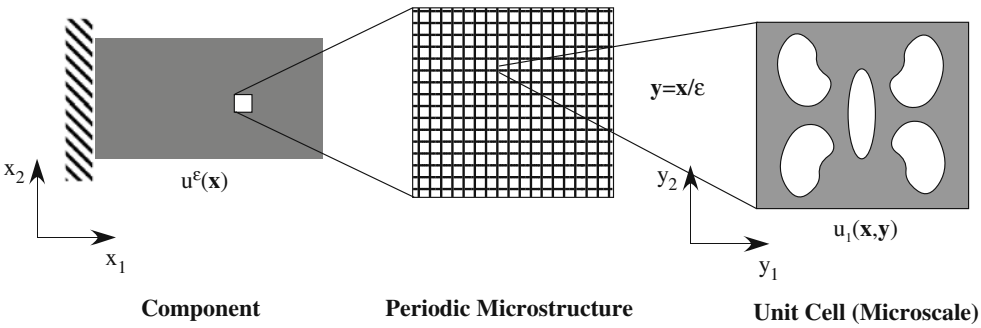

Fig. 1 Multiscale concept illustrating the macro ($\mathbf{x}$) and micro ($\mathbf{y}$) dimensions

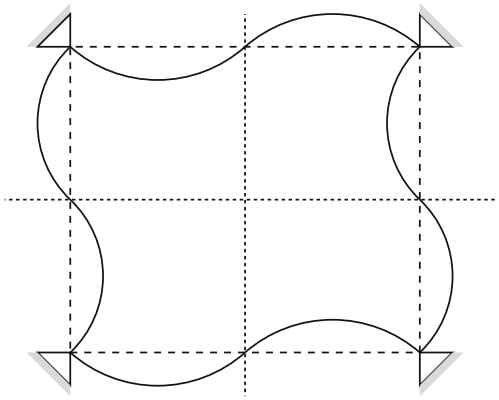

Fig. 2 Periodicity conditions in the unit cell

Therefore, substituting (6) into the microscopic equations, we obtain (Allaire 2002; Guedes and Kikuchi 1990; Sanchez-Palencia 1980):

$$\frac{1}{|Y|}\int_Y \left[\left(\mathbf{I}+\partial_y \boldsymbol{\chi}\left(\mathbf{x},\mathbf{y}\right)\right):\mathbf{D}\left(\mathbf{x},\mathbf{y}\right):\partial_y \delta\mathbf{u}_1(\mathbf{x},\mathbf{y})\right]dY=0,$$
$$\forall \delta\mathbf{u}_1 \in H_{per}(Y,R^3), \tag{8}$$

which can be rewritten using the index notation:

$$\frac{1}{|Y|}\int_Y D_{ijkl}\left(\mathbf{x},\mathbf{y}\right)\left(\delta_{im}\delta_{jn}+\frac{\partial \chi_i^{(mn)}}{\partial y_j}\right)\varepsilon_{kl}\left(\mathbf{v}\right)dY=0,$$
$$\forall \mathbf{v} \in H_{per}(Y,R^3). \tag{9}$$

Substituting (6) into the macroscopic equations, we obtain the definition of the effective properties (Allaire 2002; Guedes and Kikuchi 1990; Sanchez-Palencia 1980):

$$\mathbf{D}^H=\frac{1}{|Y|}\int_Y \left[\mathbf{D}\left(\mathbf{x},\mathbf{y}\right):\left(\mathbf{I}+\partial_y \boldsymbol{\chi}\left(\mathbf{x},\mathbf{y}\right)\right)\right]dY. \tag{10}$$

By using (8), one can easily show that (10) can also be written in the form:

$$\mathbf{D}^H=\frac{1}{|Y|}\int_Y \left[\left(\mathbf{I}+\partial_y \boldsymbol{\chi}\left(\mathbf{x},\mathbf{y}\right)\right):\mathbf{D}\left(\mathbf{x},\mathbf{y}\right):\left(\mathbf{I}+\partial_y \boldsymbol{\chi}\left(\mathbf{x},\mathbf{y}\right)\right)\right]dY, \tag{11}$$

or using the index notation:

$$D^H_{rspq}\left(\mathbf{x}\right)=\frac{1}{|Y|}\int_Y D_{ijkl}\left(\mathbf{x},\mathbf{y}\right)\left(\delta_{ip}\delta_{jq}+\frac{\partial \chi_i^{(pq)}}{\partial y_j}\right)\times\left(\delta_{kr}\delta_{ls}+\frac{\partial \chi_k^{(rs)}}{\partial y_l}\right)dY, \tag{12}$$

where $D^H_{ijkl}=D^H_{klij}=D^H_{jikl}$.

Table 1 Boundary conditions for faces (2D plane-stress)

Load cases	b.c. at $y_1=0$, $y_1=Y_1$	b.c. at $y_2=0$, $y_2=Y_2$
$m=n$ (1 or 2)	$\chi_1^{(mn)}=0;\ \sigma_{21}=0$	$\chi_2^{(mn)}=0;\ \sigma_{21}=0$
$mn=12$ (or 21)	$\chi_2^{(12)}=0;\ \sigma_{11}=0$	$\chi_1^{(12)}=0;\ \sigma_{22}=0$

The calculation of effective properties can become computationally efficient by taking advantage of symmetry boundary conditions. An isotropic unit cell has symmetry relative to all axes; and an orthotropic unit cell has symmetry relative to either both axes or only one axis. In this case, we can take advantage of these properties to reduce the computational cost and to conduct the optimization and homogenization in only one part of the domain. However, the appropriate boundary conditions must be considered for the displacement characteristic function χ. For a 2D plane-strain case, Table 1 describes the boundary conditions that must be specified when only one fourth or half of the unit cell is considered (Silva et al. 1998), as described in Figs. 3 and 4, respectively. For the half symmetry case, the actual conditions to be employed must be taken according to the type of symmetry (along x-axis as in Fig. 4 or along the y-axis).

4 Material design method

The material design optimization problem consists of finding a distribution of material inside the unit cell that will achieve specified homogenized properties. This problem is also known as the inverse homogenization problem (Cherkaev 2000; Sigmund 1994; Bendsøe and Sigmund 2003). The optimization problem consists of minimizing a cost function related to the density distribution inside the unit cell subjected to equality constraints on the elastic properties. Thus, the optimization problem can be stated in continuous form as follows (Sigmund 1994, 1995):

$$\begin{aligned}
&\underset{\rho(\mathbf{x})}{\textit{Minimize}}: \quad W(\rho)=\sum_{i,j,k,l=1}^{2} w_{ijkl}\left(D^*_{ijkl}-D^H_{ijkl}\right)^2\\
&\textit{Subjected to}: \quad \frac{1}{|Y|}\int_Y \left[\left(\mathbf{I}+\partial_y \boldsymbol{\chi}\left(\mathbf{x},\mathbf{y}\right)\right):\mathbf{D}\left(\mathbf{x},\mathbf{y}\right):\partial_y \delta\mathbf{u}_1(\mathbf{x},\mathbf{y})\right]dY=0\\
&\qquad\qquad \forall \delta\mathbf{u}_1 \in H_{per}(Y,R^3)\\
&\qquad\qquad 0\le \rho(\mathbf{x})\le 1\\
&\qquad\qquad \text{gradation control,}
\end{aligned} \tag{13}$$

where $\rho(\mathbf{x})$ is the pseudo-density distribution function along the unit cell domain, $W(\rho)$ is a cost function to

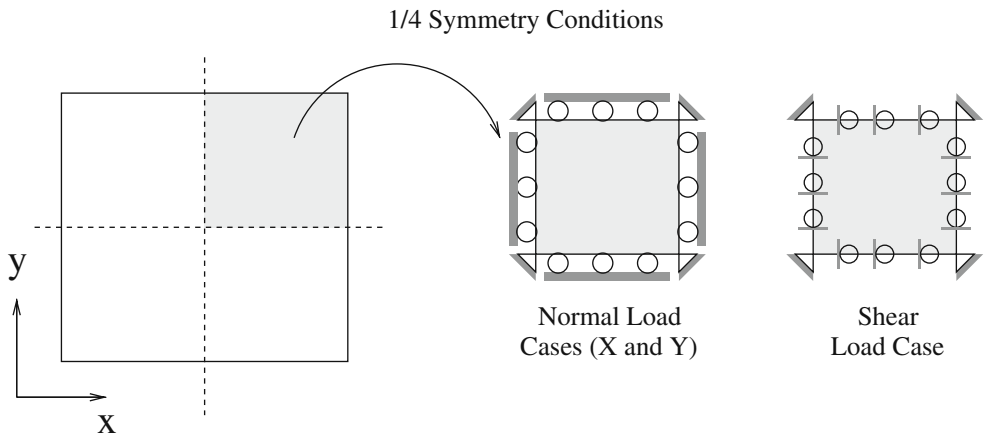

Fig. 3 Illustration of 1/4 symmetry boundary conditions for unit cell

be minimized, W is the square difference between desired and homogenized tensor properties, D^*_{ijkl} are the desired tensor properties, D^H_{ijkl} are the homogenized tensor properties, and w_{ijkl} are weight coefficients to control the proximity between desired and homogenized tensor property. Here emphasis is placed in 2D problems, thus the indices i, j, k, and l range from 1 to 2. The gradation control constraint is used to adjust the material gradation, which is a key point in this work. The gradation control constraint also improves aspects associated to mesh dependency and numerical instabilities of the Continuous Approximation of Material Distribution (CAMD) approach such as the "islands" phenomenon (Matsui and Terada 2004). The implementation of the gradation control constraint is described in the Subsection 6.3.

5 A material model

This work is concerned with FGMs represented by the transition between two basic materials. The objective is to find the optimal volume fraction of this mixture at each point of the domain, so that the FGM property gradation inside the unit cell can also be found. To achieve this, we will allow for intermediate materials (no penalization), and to guarantee that the final composite can be achieved by a mixture of the chosen basic materials, a material model based on the Hashin and Shtrikman (H–S) bounds is employed (Hashin and Shtrikman 1963; Cherkaev and Gibiansky 1993; Bendsøe and Sigmund 2003). These bounds provide the range of effective properties achievable for a certain volume fraction of the mixture of two isotropic materials.

Thus, considering the upper and lower limits of bulk modulus (K) and shear modulus (G) properties, the material model is defined as (Bendsøe and Sigmund 2003):

$$K^m(\rho) = \kappa K_{\max}(\rho) + (1-\kappa) K_{\min}(\rho) \tag{14}$$

$$G^m(\rho) = \kappa G_{\max}(\rho) + (1-\kappa) G_{\min}(\rho), \tag{15}$$

where ρ is the pseudo-density describing the amount of material at each point of the domain, which can assume values between 0 and 1. The parameters K^m and G^m are the bulk and shear modulus of the mixture, respectively; $K_{\max}$, $G_{\max}$ and $K_{\min}$, $G_{\min}$ are the upper and lower limits of these moduli, and they are given by (53) through (56) in the Appendix A. The parameter κ

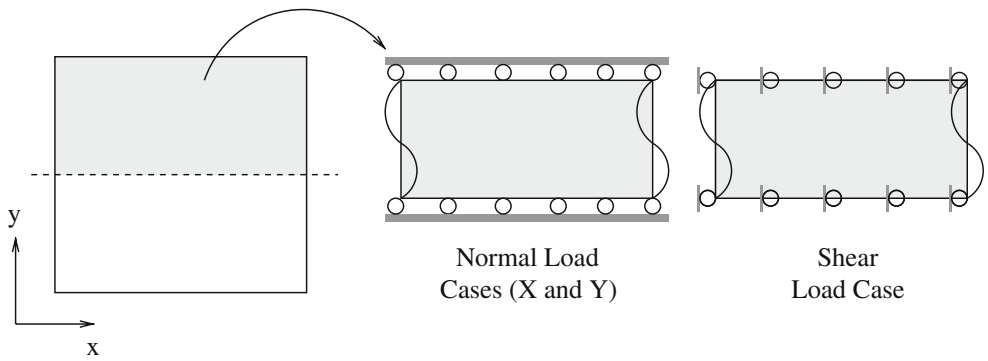

Fig. 4 Illustration of 1/2 symmetry boundary conditions for unit cell

is an interpolation factor to define a curve interpolating the upper and lower limits of bulk and shear modulus. In this work, $\kappa = 0.5$. The basic materials of the mixture will be designated by the symbols (+) and (−). They have bulk and shear modulus equal to K^+, K^- and G^+, G^-, respectively, such that $K^+ > K^-$ and $G^+ > G^-$. The values of $K_{\max}$, $K_{\min}$, $G_{\max}$, and $G_{\min}$ are functions of those properties (Appendix A). For ρ equal to 0 the material is equal to material (−) and for ρ equal to 1 it is equal to material (+).

The Young's modulus (E^m) and Poisson's ratio (ν^m) of the mixture can be written as a function of K^m and G^m through the expressions:

$$E^m(\rho) = \frac{9K^m(\rho)}{1 + 3\frac{K^m(\rho)}{G^m(\rho)}}; \quad \nu^m(\rho) = \frac{1 - 2/3\frac{G^m(\rho)}{K^m(\rho)}}{2 + 2/3\frac{G^m(\rho)}{K^m(\rho)}}. \tag{16}$$

Regarding the capability of traditional micromechanical models to evaluate effective properties, Reiter et al. (1997) have investigated the Mori-Tanaka and Self-consistent models to estimate these properties. Their main conclusion is that these models can be applied to the regions where the inclusion and the matrix phases can be easily distinguished. For the transition region, these models may be valid depending on the ratio of phase properties.

The use of traditional micromechanical models for FGMs has been questioned in the literature because the continuous transition of microstructure causes a non-uniform macroscopic distribution of properties. Thus traditional approaches have limitations, and the reader is referred to the technical literature in the subject (Pindera et al. 1995; Yin et al. 2004). The computational framework presented here is general, and thus other material models can easily replace the present one based on H-S bounds (which assumes that the FGM gradation law is smooth enough for its application).

6 Numerical implementation

The concept of the continuum distribution of design variable based on the CAMD method (Matsui and Terada 2004; Rahmatalla and Swan 2004) discussed above is considered. Thus, (14) and (15) are considered for each node, and the pseudo-density (ρ) inside each finite element is given by

$$\rho(\mathbf{x}) = \sum_{I=1}^{n_d} \rho_I N_I, \tag{17}$$

where ρ_I is the nodal design variable, N_I is the finite element shape function that must be selected to provide non-negative values of the design variables, and n_d is the number of nodes at each element (for example, four in the 2D case). This formulation allows a continuous distribution of material along the design domain instead of the traditional piecewise constant material distribution applied by previous formulations of topology optimization (Bendsøe and Sigmund 2003).

6.1 Homogenization

The numerical implementation of homogenization is presented considering the CAMD concept. Equation (8) is solved using FEM. The unit cell is discretized by N finite elements, thus:

$$Y = \cup_{e=1}^{N} \Omega^e, \tag{18}$$

where Ω^e is the domain of each element. A four-node bilinear element with two displacements degrees of freedom per node that uses bilinear interpolation functions was applied. Thus, the characteristic functions previously defined are expressed at each element using the shape functions (N_I):

$$\chi_i^{(mn)} \cong \sum_{I=1}^{n_d} N_I \chi_{iI}^{(mn)}, \tag{19}$$

Similar relations hold for the virtual displacement $\mathbf{v}$. Substituting (19) in (8), and assembling the individual matrices for each element, we obtain the following global matrix system for each load case mn:

$$\mathbf{K}\widehat{\boldsymbol{\chi}}^{(mn)} = \mathbf{F}^{(mn)}, \tag{20}$$

where $\widehat{\boldsymbol{\chi}}^{(mn)}$ are the corresponding nodal values of the characteristic function $\boldsymbol{\chi}$, respectively. The global stiffness is the assembly of each element's individual matrix, and the global force ($\mathbf{F}$) is the assembly of the individual force vectors for all elements.

$$\mathbf{K} = A_{e=1}^{N} \mathbf{K}^e; \quad \mathbf{F}^{(mn)} = A_{e=1}^{N} \mathbf{F}^{e(mn)}. \tag{21}$$

The element matrices and vectors are given by the expressions:

$$K^e_{(iIjJ)} = \int_{\Omega^e} D_{ipjq} \frac{\partial N_I}{\partial y_p} \frac{\partial N_J}{\partial y_q} d\Omega^e;$$
$$F_{iI}^{e(mn)} = \int_{\Omega^e} D_{ijmn} \frac{\partial N_I}{\partial y_j} d\Omega^e. \tag{22}$$

Thus, for the 2D problem, there are three load cases to be solved independently as illustrated in Fig. 5. They

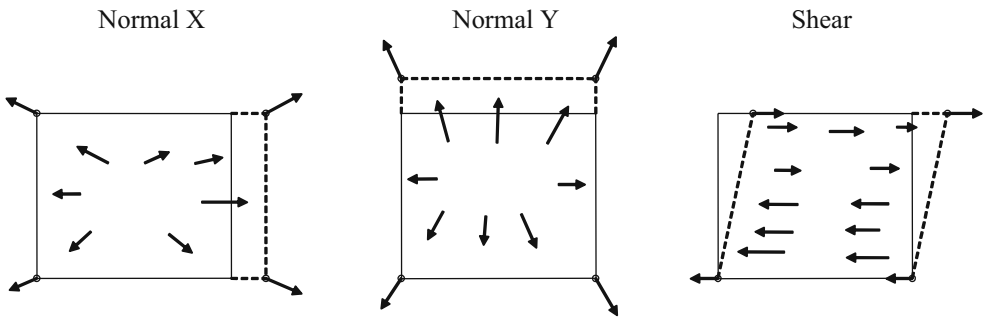

Fig. 5 Schematic illustration of applied load cases to the unit cell with associated material forces

come from (20), where the indices m and n can be 1 or 2, resulting in the combinations "11", "22", and "12" or "21". All load cases must be solved by enforcing periodic boundary conditions in the unit cell for the displacements (see Fig. 2).

The unit cell is made of an FGM material. The material properties change gradually inside the element domain, and thus, the material property must be kept inside of the integral during integration using the graded finite element concept (Kim and Paulino 2002) (see Fig. 6). An order 2 Gaussian rule in each direction is applied to calculate integrals (22) and (11) for computing the effective properties.

Regarding the numerical solution of the matrix system (20), the total matrix bandwidth is spoiled due to enforcement of periodicity conditions. This increases the amount of memory storage necessary for the matrix. This problem can be avoided when the unit cell is symmetric. In this case, we consider the symmetry boundary conditions described in Table 1, instead of the periodicity conditions.

The displacements at some point of the unit cell must be prescribed to overcome the non-unique solution of the problem, otherwise the FEM problem will be ill-posed. The choice of this point with prescribed values does not affect the homogenized coefficients because only the derivatives of the characteristic functions are used in their computation.

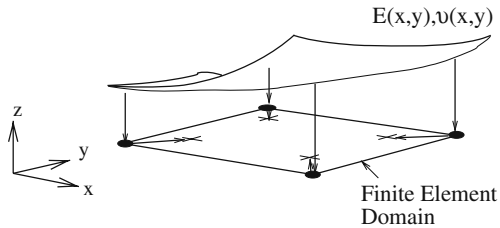

Fig. 6 Continuous material distribution using a graded finite element

6.2 Material design problem

The material design problem can be stated in a discrete form considering a two dimensional (2D) finite element domain:

$$\begin{aligned} &\underset{\rho_I}{\textit{Minimize}}: && W(\rho_I) = \textstyle\sum_{m,n=1}^{2} w_{mn}\left(D^{*}_{mn}(\rho_I)\right. \\ &&& \left. - D^{H}_{mn}(\rho_I)\right)^2 \\ &\textit{Subjected to}: && \mathbf{K}\widehat{\boldsymbol{\chi}}^{(mn)} = \mathbf{F}^{(mn)} \\ &&& 0 \le \rho_I \le 1 \qquad I = 1..NDV \\ &&& \text{gradation control,} \end{aligned} \tag{23}$$

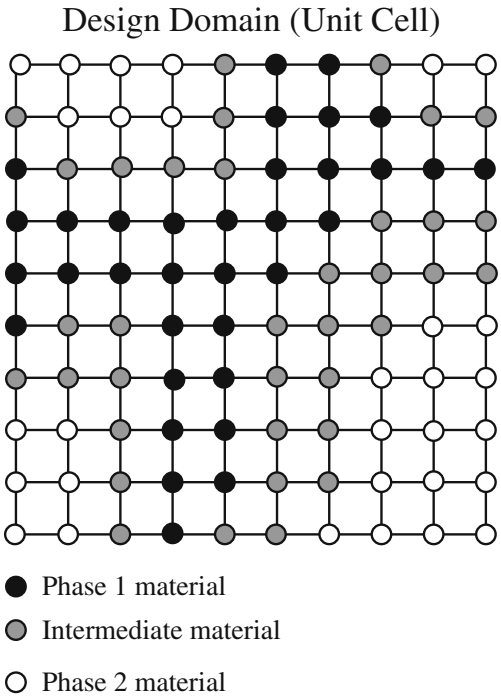

Fig. 7 Design domain—note that pseudo-densities are defined for each node

where ρ_I is the design variable (pseudo-density) that represents the fraction of material at each finite element node of the design domain (see Fig. 7). There are NDV design variables, NDV being equal to the total number of finite elements N less the number of elements that are explicitly excluded from the optimization ($NEXCL$). If the basic isotropic material ($-$) is void ($E^- = 0$) than a lower bound ρ_{low} must be specified for design variables ρ_I, to avoid numerical problems (singularity of the stiffness matrix in the finite element formulation). Numerically, regions with $\rho_I = \rho_{low}$, have practically no structural significance and can be considered void regions. In this work, the value for ρ_{low} is equal to 10^{-7}. Regarding the constraint related to the symmetry conditions, and considering the design domain a rectangular (2D problem) unit cell, we can define many kinds of symmetries relative to the symmetry axes of the rectangular domain. In this work, two symmetry axes are considered to reduce the computational cost as only one-quarter of the unit cell is used as a design domain. The symmetry conditions are implicitly expressed in the boundary conditions during the homogenization, as described in Section 3.

A flow-chart of the optimization algorithm is shown in Fig. 8. The design variables are the pseudo-densities, which can assume different values at each finite element node. Four node bilinear isoparametric elements considering plane stress formulation are used in the finite element formulation (e.g. Kim and Paulino 2002). The optimization problem is solved by using the MMA algorithm which handles a relatively large number of design variables (Svanberg 1987; Bruyneel et al. 2002). The algorithm requires the sensitivities which are derived in Section 7. The iteration must start with a random initial guess of ρ_I distribution. The initial values for the design variables cannot be uniform (homogeneous material) because they would generate equal values of gradients in relation to all design variables, and thus, the optimization method would not have a preferential direction for starting the search. As expected, the problem is highly dependent on the initial guess (Sigmund 1994, 1995; Sigmund and Torquato 1997).

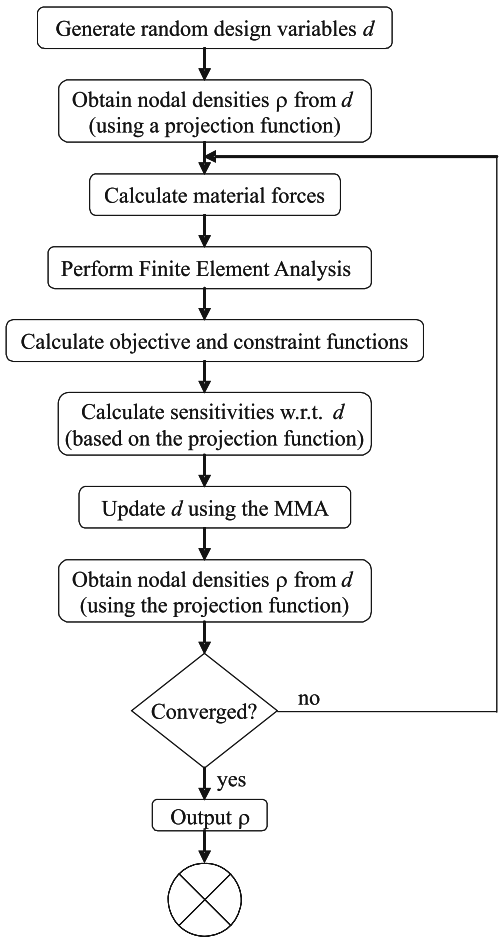

Fig. 8 Flow-chart of the optimization procedure

6.3 Material gradation control

The CAMD approach ensures a continuous material distribution across elements. However, it does not provide a general control of the gradient of material distribution. To achieve a mesh-independent control of the gradient of material distribution, we introduce a new layer of design variables and use a projection function to obtain the material densities at nodes. The use of nodal design variables and projection functions (Guest et al. 2004) will be applied on top of the CAMD in this paper (Carbonari et al. 2007).

Let d_n denote all design variables associated with nodes, and ρ_n, all values of material density at nodes. Assume that the required change of material density must occur over a minimum length of r_{min}. By means of the projection function (f), ρ_n can be obtained from d_n as follows (assuming that four-node element is used)

$$\rho_n = f(d_n), \tag{24}$$

where f is the projection function

$$\rho_i = f(d_j) = \frac{\sum_{j \in S_i} d_j \, w(r_{ij})}{\sum_{j \in S_i} w(r_{ij})}, \tag{25}$$

and r_{ij} is the distance between nodes j and i

$$r_{ij} = \left\| \mathbf{x}_j - \mathbf{x}_i \right\|. \tag{26}$$

and S_i is the set of nodes in the domain under influence of node i, which consists of a circle of radius r_{min} and center at node i. The weight function w is defined as follows.

$$w\left(r_{ij}\right) = \begin{cases} \frac{r_{min}-r_{ij}}{r_{min}} & \text{if } \mathbf{x}_j \in S_i \\ 0 & \text{otherwise} \end{cases}, \tag{27}$$

Figure 9 illustrates the idea of the projection technique.

The topology optimization problem definition is revised as follows.

$$\begin{aligned} \underset{d_I}{Minimize}: \quad & W\left(d_I\right) = \sum_{m,n=1}^{2} w_{mn}\left(D^{*}_{mn}\left(d_I\right) - D^{H}_{mn}\left(d_I\right)\right)^2 \\ Subjected\ to: \quad & \mathbf{K}\widehat{\boldsymbol{\chi}}^{(mn)} = \mathbf{F}^{(mn)} \\ & 0 \le f\left(d_I\right) \le 1 \qquad I = 1..NDV \\ & \text{gradation control.} \end{aligned} \tag{28}$$

Sensitivities with respect to design variables are obtained based on those with respect to nodal densities using chain-rule

$$\frac{\partial\left(.\right)}{\partial d_i} = \sum_{j\in\Omega} \frac{\partial\left(.\right)}{\partial \rho_j}\frac{\partial \rho_j}{\partial d_i}, \tag{29}$$

where Ω is the entire domain, but $\partial\rho_j/\partial d_i$ is non-zero only at nodes j whose influence domain (S_j) contains node i. Moreover

$$\frac{\partial \rho_j}{\partial d_i} = \frac{w(r_{ij})}{\sum_{k\in S_j} w(r_{kj})}. \tag{30}$$

where $\partial\left(.\right)/\partial\rho_j$ is obtained by using traditional methods such as the adjoint method, as described in the next section.

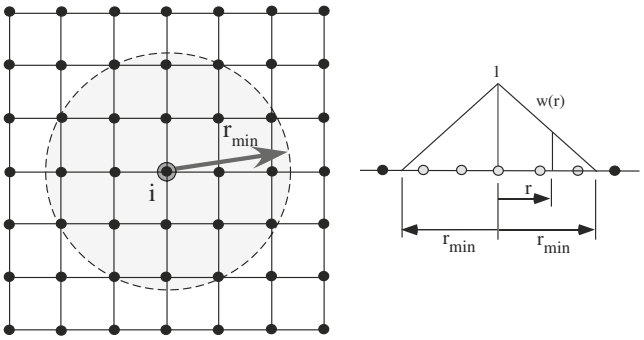

Fig. 9 Projection technique concept

7 Sensitivity analysis

To solve the optimization problem defined above, it is necessary to calculate the sensitivity of objective function and constraints in relation to the design variables. The sensitivities of the homogenized properties are well-known in the literature (Sigmund 1994, 1995), however, here the formulation is described considering the CAMD concept.

Differentiating (11) in relation to the design variable and considering (8), after some algebraic manipulation, we get (Sigmund 1994; Sigmund and Torquato 1997):

$$\frac{\partial \mathbf{D}^H}{\partial \rho_I} = \frac{1}{|Y|}\int_Y \left[\left(\mathbf{I} + \partial_y \boldsymbol{\chi}\left(\mathbf{x},\mathbf{y}\right)\right) : \frac{\partial \mathbf{D}^m\left(\mathbf{x},\mathbf{y}\right)}{\partial \rho_I} : \left(\mathbf{I} + \partial_y \boldsymbol{\chi}\left(\mathbf{x},\mathbf{y}\right)\right)\right] dY. \tag{31}$$

However, considering the material models, given by (14) and (15),

$$\frac{\partial \mathbf{D}^m\left(\mathbf{x},\mathbf{y}\right)}{\partial \rho_I} = \frac{\partial \mathbf{D}^m\left(\mathbf{x},\mathbf{y}\right)}{\partial \rho}\frac{\partial \rho}{\partial \rho_I}, \tag{32}$$

and the continuous distribution of the design variable given by (17) inside each finite element is

$$\rho\left(\mathbf{x}\right) = \sum_{I=1}^{n_d} \rho_I N_I \Longrightarrow \frac{\partial \rho}{\partial \rho_I} = N_I(\mathbf{x}). \tag{33}$$

By discretizing the domain into finite elements, the above integral will include all m_I elements associated with I-th node, thus:

$$\frac{\partial \mathbf{D}^H}{\partial \rho_I} = \frac{1}{|Y|}\sum_{e=1}^{m_I}\left[\int_{\Omega^e}\left[\left(\mathbf{I} + \partial_y \boldsymbol{\chi}\left(\mathbf{x},\mathbf{y}\right)\right) : N_I(\mathbf{x})\frac{\partial \mathbf{D}^m\left(\mathbf{x},\mathbf{y}\right)}{\partial \rho} : \left(\mathbf{I} + \partial_y \boldsymbol{\chi}\left(\mathbf{x},\mathbf{y}\right)\right)\right] d\Omega^e\right]. \tag{34}$$

The calculation of gradients is straightforward and fast (low computational cost) which contributes to the efficiency of the optimization. The calculation of sensitivity $\partial\mathbf{D}^m\left(\mathbf{x},\mathbf{y}\right)/\partial\rho$ is described in Appendix B. In the case of plane stress, the tensor properties $\mathbf{D}^m$ for a two-dimensional problem is given by

$$\mathbf{D}^m = \frac{E^m}{1-(v^m)^2}\begin{bmatrix} 1 & v^m & 0 \\ v^m & 1 & 0 \\ 0 & 0 & \frac{1-v^m}{2} \end{bmatrix}. \tag{35}$$

8 Results

To illustrate the theoretical and numerical approaches, numerical examples are provided. The homogenization method is verified by considering one-dimensional material gradation profiles for which analytical solutions for the effective elastic properties are available. The verification of the homogenization method is also extended to two dimensions considering a trigonometric material gradation, and a material variation with discontinuous derivatives. These are also used as benchmark examples to verify the optimization method for FGM cell design. Finally the influence of material gradation on extreme materials is investigated, which includes materials with near-zero shear modulus, and materials with negative Poisson's ratio. The examples provided are listed below:

- Verification of homogenization for one-dimensional gradation
- Homogenization of two-dimensional FGM unit cells
    1. Trigonometric material gradation
    2. Material with discontinuous derivatives
- Optimized FGM cell design
    1. Trigonometric material gradation
    2. Material with discontinuous derivatives
    3. Near-zero shear modulus materials
    4. Negative Poisson's ratio materials

The material design requires the volume fraction of material in the optimization process. The averaged volume fraction is defined by the expression:

$$\Theta = \int_{\Omega} \rho d\Omega \Longrightarrow \Theta \cong \sum_{i=1}^{NDV} \rho_i V_i, \tag{36}$$

where Vi is the relative volume of each finite element in the unit cell.

8.1 Verification for one-dimensional gradation

To verify the numerical implementation of the homogenization method for FGM composites, a two-dimensional (2-D) problem with one-dimensional gradation will be considered ($\mathbf{Y} = [0, 1]$), so that analytical results of the effective properties can be obtained. To ensure that the FGM can be obtained by a mixture of two materials, the FGM gradation is defined for the pseudo-density (ρ) and the properties at each point of the domain are obtained using the H-S bounds (see Appendix A). The (idealized) gradation is given by

$$\rho(x) = (\cos 2\pi x + 1)/2 \quad \text{and} \quad 0 \le x \le 1, \tag{37}$$

with $E^+ = 8$, $\nu^+ = 0.3$, and $E^- = 1$, $\nu^- = 0.3$.

From reference (Bendsøe and Sigmund 2003), the effective elastic properties for this type of composite can be obtained by solving the analytical expressions:

$$D_{11}^H = \frac{1}{\int_0^1 \frac{1}{D_{11}} dx}; \qquad D_{12}^H = \frac{\int_0^1 \frac{D_{12}}{D_{11}} dx}{\int_0^1 \frac{1}{D_{11}} dx}$$

$$D_{22}^H = \int_0^1 D_{22} dx - \int_0^1 \frac{D_{12}^2}{D_{11}} dx + \frac{\left(\int_0^1 \frac{D_{12}}{D_{11}} dx\right)^2}{\int_0^1 \frac{1}{D_{11}} dx};$$

$$D_{33}^H = \frac{1}{\int_0^1 \frac{1}{D_{33}} dx}. \tag{38}$$

Thus, by computing the above integrals, the following effective properties are readily obtained:

$$\mathbf{D}^H = \begin{bmatrix} 1.817 & 0.554 & 0 \\ 0.554 & 2.460 & 0 \\ 0 & 0 & 0.632 \end{bmatrix}. \tag{39}$$

To solve the homogenization equations by the FEM, a mesh convergence analysis was performed. The results of Fig. 10 show that a mesh of 22×22 provides converged values for the material property values:

$$\mathbf{D}^H = \begin{bmatrix} 1.818 & 0.555 & 0 \\ 0.555 & 2.462 & 0 \\ 0 & 0 & 0.632 \end{bmatrix}. \tag{40}$$

with accuracy less than 0.1%.

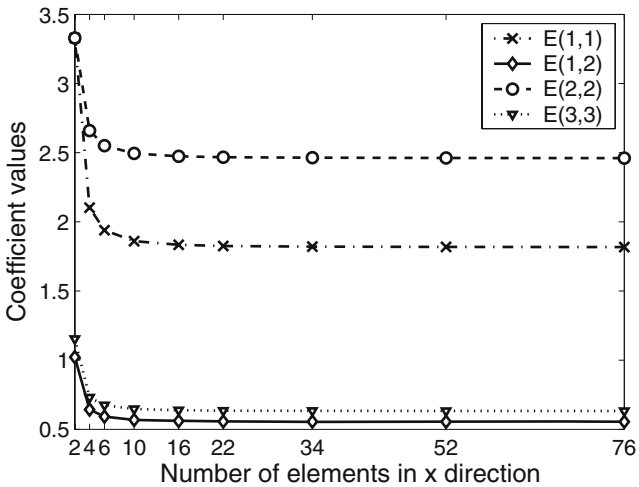

Fig. 10 Convergence analysis for homogenized properties

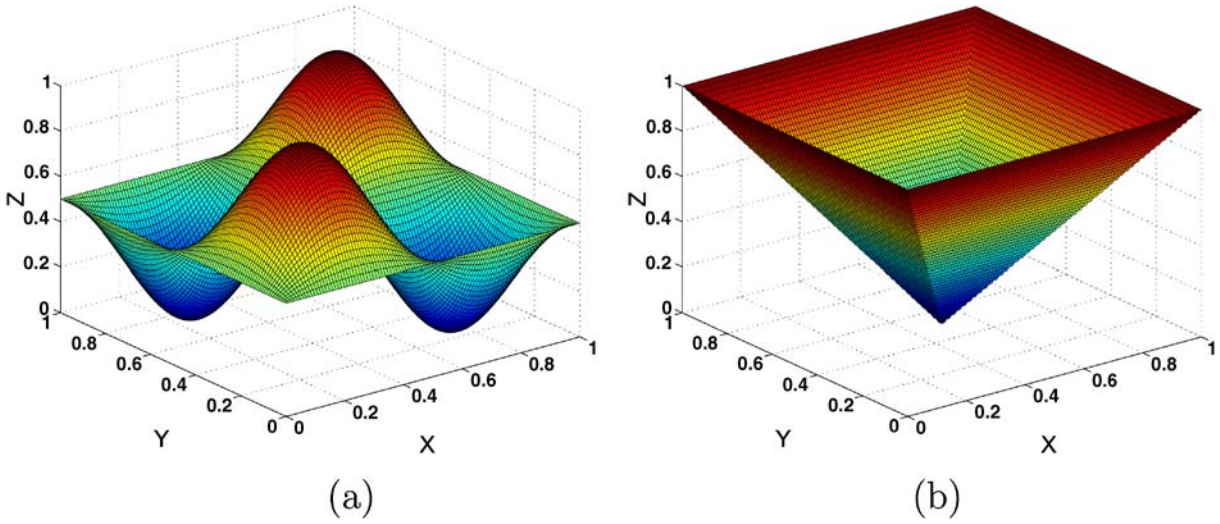

Fig. 11 **a** Trigonometric material gradation; **b** material with discontinuous derivatives

8.2 Homogenization of FGM unit cells

To illustrate the potentiality of the method, some two-dimensional (2-D) FGM composite unit cells ($\mathbf{Y} = [0, 1] \times [0, 1]$) with two-dimensional gradation were homogenized. The same homogenized properties were used as input for the material design problem in Section 4 to check its capability to recover the material distribution.

8.2.1 Example 1 – trigonometric material gradation

The first gradation law considered (for the pseudo-density) is given by:

$$\rho(x, y) = (\sin 2\pi x \ \sin 2\pi y + 1)/2 \ \text{ and}$$
$$0 \le x \le 1; 0 \le y \le 1. \tag{41}$$

as shown in Fig. 11a.

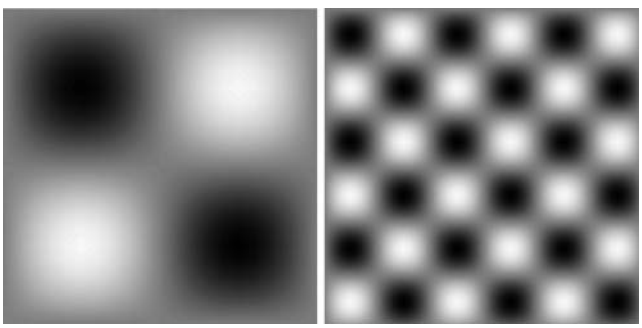

Fig. 12 Benchmark material with trigonometric gradation. **a** Pseudo-density distribution in the unit cell; **b** corresponding composite material matrix

Figure 12a and b describe the pseudo-density distribution in the unit cell and the corresponding composite material matrix. The calculated effective property values using a 40×40 mesh are

$$\mathbf{D}^H = \begin{bmatrix} 2.7148 & 0.9180 & 0 \\ 0.9180 & 2.7148 & 0 \\ 0 & 0 & 1.0266 \end{bmatrix}. \tag{42}$$

8.2.2 Example 2—material with discontinuous derivatives

The second gradation law considered (for the pseudo-density) is given by:

$$\rho(x, y) = \begin{cases} 1 - 2x \ \text{ and } 0 \le x \le 1/2; & x \le y \le 1 - x \\ 2x - 1 \ \text{ and } \ 1/2 \le x \le 1; & 1 - x \le y \le x \\ 1 - 2y \ \text{ and } 0 \le y \le 1/2; & y \le x \le 1 - y \\ 2y - 1 \ \text{ and } \ 1/2 \le y \le 1; & 1 - y \le x \le y \end{cases}. \tag{43}$$

as shown in Fig. 11b.

Notice that this gradation does not have continuous derivatives. Figure 13a and b describe the pseudo-density distribution in the unit cell and the corresponding composite material matrix. The calculated effective property values using a 40×40 mesh are

$$\mathbf{D}^H = \begin{bmatrix} 4.0457 & 1.1507 & 0 \\ 1.1507 & 4.0457 & 0 \\ 0 & 0 & 1.2954 \end{bmatrix}. \tag{44}$$

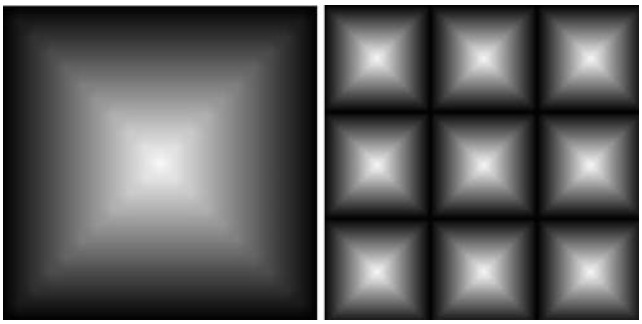

(a) (b)

Fig. 13 Benchmark material with discontinuous derivative. **a** Pseudo-density distribution in the unit cell; **b** corresponding composite material matrix

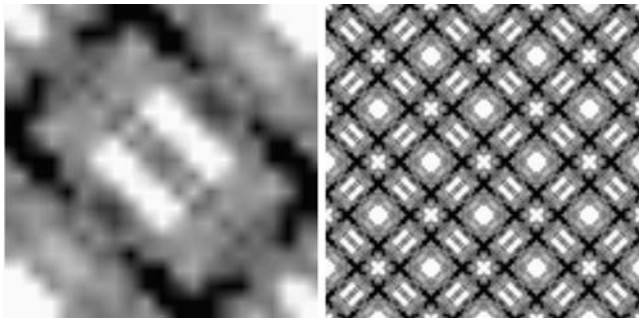

(a) (b)

Fig. 15 Topology optimization result (trigonometric gradation) without gradient control. **a** Unit cell pseudo-density distribution; **b** corresponding composite material matrix. Notice that the lack of gradient control leads to undesirable results (e.g. local minimum)

8.3 Optimized FGM cell design

Material design examples, using the implemented software, are presented. Unless otherwise specified, a square design domain with four symmetry axes (horizontal, vertical, and both diagonals) is adopted (see Fig. 3). The symmetry ensures that the obtained composite material will be orthotropic with equal values for properties D_{11} and D_{22}. The same property values for the basic materials (+) and (−), adopted in Section 8.2, are used here. The coefficients w_{11}, w_{22}, w_{12}, and w_{33} adopted for the objective function in problem (23) are equal to 1, 1, 5, and 15, respectively. These values were chosen after some numerical experiments. A large value was chosen for the shear coefficient because it is the most difficult one to match in the problem (13). In traditional material design for composites, some discussion about the influence of weight coefficients can be found in references (Sigmund 2000; Gibiansky and Sigmund 2000).

8.3.1 Example 1—trigonometric material gradation

The first material design example consists of trying to recover the unit cell pattern presented in Example 1 of Section 8.2. Thus, the effective properties in (42) are specified as desired properties in the objective function of problem (23). The unit cell design domain is discretized into 20 × 20 finite elements. Initially, the gradient control with r_{min} equal to 0.318 was applied. This value is based on the pseudo-density distribution of (41). Figure 14a and b show the obtained pseudo-density distribution in the unit cell and the corresponding composite material matrix. The following property values were obtained from the optimization problem:

$$\mathbf{D}^H = \begin{bmatrix} 2.7147 & 0.9192 & 0 \\ 0.9192 & 2.7147 & 0 \\ 0 & 0 & 1.0262 \end{bmatrix}. \tag{45}$$

which are similar to the ones in expression (42).

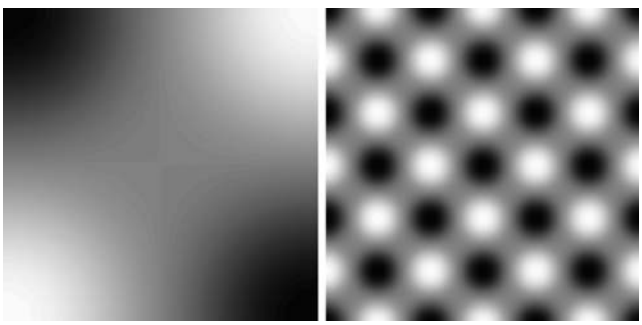

(a) (b)

Fig. 14 Topology optimization result (trigonometric gradation) with gradient control; **a** Unit cell pseudo-density distribution; **b** corresponding composite material matrix

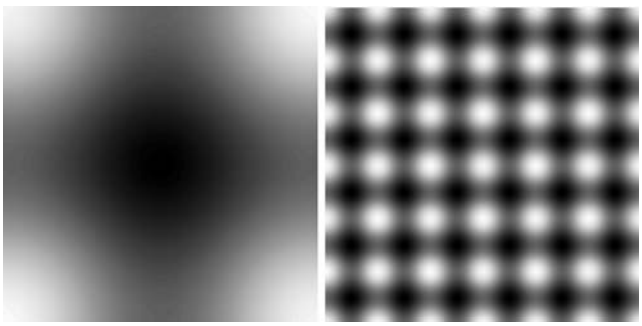

(a) (b)

Fig. 16 Topology optimization result (benchmark material with discontinuous derivative) with gradient control. **a** Unit cell pseudo-density distribution; **b** corresponding composite material matrix

Notice that the recovered pattern shown in Fig. 14b is similar to the original one shown in Fig. 12b. Quantitavely, the averaged volume fraction (Θ) of the recovered pattern for material (+) is equal to 0.5, exactly the same value for the original pattern.

If no gradient control is used, the results shown in Figs. 15a and b are obtained, which are different from the original pattern shown in Fig. 12a and b, and the following property values are obtained:

$$\mathbf{D}^H = \begin{bmatrix} 2.7147 & 0.9173 & 0 \\ 0.9173 & 2.7147 & 0 \\ 0 & 0 & 1.0267 \end{bmatrix}. \quad (46)$$

These results are similar to the ones in expressions (42) and (45). However, in this case, the averaged volume fraction of the recovered pattern is equal to 0.483, which is different from the original pattern. *This example shows that the use of gradient control is quite significant for designing FGM microstructures*.

8.3.2 Example 2—material with discontinuous derivatives

This example consists of recovering the unit cell pattern of Example 2 presented in Section 8.2. Thus, the effective properties in (44) are specified as desired properties in the objective function of problem (23). The same design domain as the previous example is adopted.

Initially, the gradient control with r_{min} equal to 0.5 was applied. Figure 16a and b show the pseudo-density distribution in the unit cell and the corresponding composite material matrix. The following properties were obtained from the optimization problem:

$$\mathbf{D}^H = \begin{bmatrix} 3.9669 & 1.1735 & 0 \\ 1.1735 & 3.9669 & 0 \\ 0 & 0 & 1.3204 \end{bmatrix}. \quad (47)$$

which are similar to the ones in expression (44).

In the original pattern, the material gradation derivatives are not continuous. Thus, by using gradient control we cannot expect to recover the same pattern as shown in Fig. 13a and b. However, the method provides the best solution close to the desired one in the minimum square sense. Quantitatively, the averaged

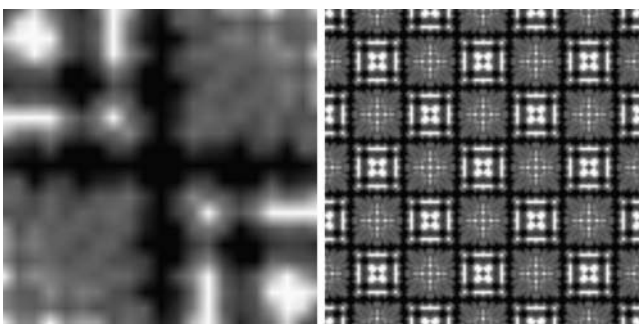

(a) (b)

Fig. 17 Topology optimization result (benchmark material with discontinuous derivative) without gradient control. **a** Unit cell pseudo-density distribution; **b** corresponding composite material matrix. Again, the lack of gradient control leads to undesirable results (e.g. local minimum)

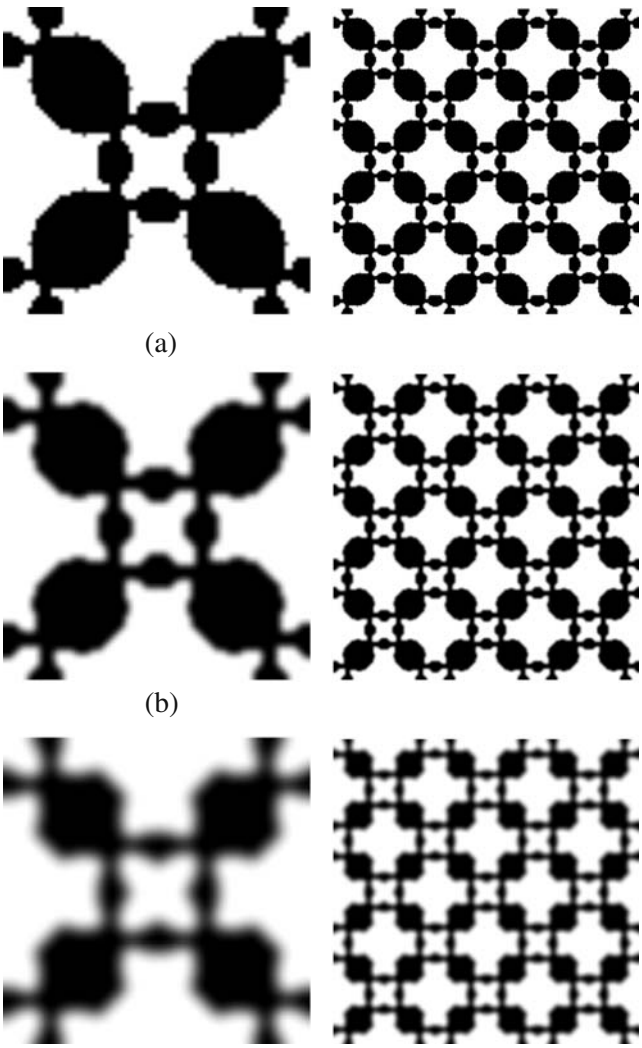

(a) (b) (c)

Fig. 18 Unit cell pseudo-density distribution and corresponding composite material matrix for a material with near zero shear modulus: **a** $r_{min} = 1$, $\Theta = 43.4\%$; **b** $r_{min} = 2$, $\Theta = 36.1\%$; **c** $r_{min} = 4$, $\Theta = 25.4\%$

volume fraction of the recovered pattern for material (+) is equal to 0.658, while for the original pattern is 0.666.

If no gradient control is used, the results in Fig. 17a and b are obtained, which are different from the original pattern shown in Fig. 13a and b, however, it recovers the property values ((44) and (47)):

$$\mathbf{D}^H = \begin{bmatrix} 4.045 & 1.1510 & 0 \\ 1.1510 & 4.045 & 0 \\ 0 & 0 & 1.2951 \end{bmatrix}. \tag{48}$$

The average volume fraction of the recovered pattern is equal to 0.649, which is different from the original pattern (0.666). As expected, the FGM gradation imposes additional constraints in the material design process, which means that not all property values that could be feasible in a unit cell design without this constraint, can be obtained.

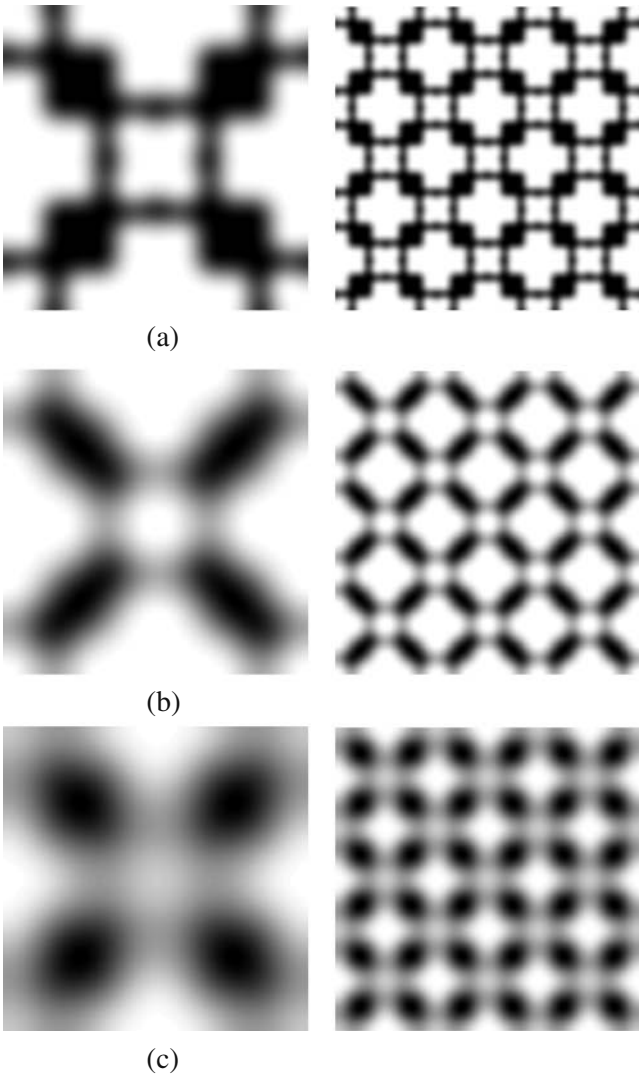

Fig. 19 Unit cell pseudo-density distribution and corresponding composite material matrix for a material with near zero shear modulus: **a** $r_{min} = 6$, $\Theta = 19.5\%$; **b** $r_{min} = 10$, $\Theta = 11.3\%$; **c** $r_{min} = 20$, $\Theta = 13.4\%$

8.3.3 Example 3—near zero shear modulus

The objective of this example is to analyze the influence of FGM gradation in the design of extreme materials. It is known that extreme materials can only be obtained with solid-void (0–1) designs and steep material variation (Sigmund 2000). However, usually, some gradation is obtained in the manufacturing processes of such materials. Thus, the question is how this gradation influences the behavior of a designed extreme material. To illustrate this point, we consider the design of materials with zero shear modulus and negative Poisson's ratio. First, the design of a material with zero shear modulus is considered.

Such material consists essentially of a mechanism, thus in the case of material design there will be always a minimum value for the shear modulus. The prescribed properties are

$$\mathbf{D} = \begin{bmatrix} 1.0 & 1.0 & 0 \\ 1.0 & 1.0 & 0 \\ 0 & 0 & 0.0 \end{bmatrix}. \tag{49}$$

In this problem, Young's modulus, E^+ and E^-, and Poisson's ratio, ν^+ and ν^-, of basic materials are equal to 27.3, 0.0, 0.3, and 0.0, respectively. The unit cell design domain is discretized into 40×40 finite elements. The unit cell designs for r_{min} equal to 1 (no gradation), 2, 4; 6, 10, and 20 are shown in Figs. 18 and 19. The corresponding computed property values are described below:

$$\mathbf{D}^H\left(r_{min}=1\right) = \begin{bmatrix} 1.0356 & 0.9662 & 0 \\ 0.9662 & 1.0356 & 0 \\ 0 & 0 & 0.0324 \end{bmatrix}$$

$$\mathbf{D}^H\left(r_{min}=2\right) = \begin{bmatrix} 1.0549 & 0.9412 & 0 \\ 0.9412 & 1.0549 & 0 \\ 0 & 0 & 0.0602 \end{bmatrix}$$

$$\mathbf{D}^H\left(r_{min}=4\right) = \begin{bmatrix} 1.0064 & 0.8593 & 0 \\ 0.8593 & 1.0064 & 0 \\ 0 & 0 & 0.1463 \end{bmatrix}$$

$$\mathbf{D}^H\left(r_{min}=6\right) = \begin{bmatrix} 1.0357 & 0.7493 & 0 \\ 0.7493 & 1.0357 & 0 \\ 0 & 0 & 0.1688 \end{bmatrix}$$

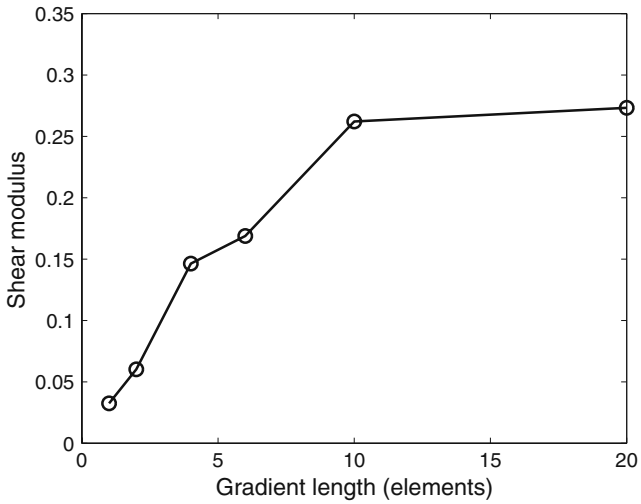

Fig. 20 Shear modulus as a function of r_{min} (gradient length)

$$\mathbf{D}^H\left(_{r_{min}=10}\right) = \begin{bmatrix} 0.9453 & 0.5210 & 0 \\ 0.5210 & 1.0255 & 0 \\ 0 & 0 & 0.2621 \end{bmatrix}$$

$$\mathbf{D}^H\left(_{r_{min}=20}\right) = \begin{bmatrix} 0.8505 & 0.2903 & 0 \\ 0.2903 & 0.9960 & 0 \\ 0 & 0 & 0.2732 \end{bmatrix}. \quad (50)$$

As r_{min} increases, the recovered properties differ from the specified ones in (49). The plot of the shear modulus value as a function of r_{min} (gradient length) is shown in Fig. 20. It is noticed that the shear modulus does not change significantly after r_{min} =10. The difference between each of the above cases and the reference property of (49) in the max norm is 3.4%, 6%, 14.6%, 25.1%, 47.9%, 71%, respectively. Moreover, one observes that the solution degrades when imposing gradient control.

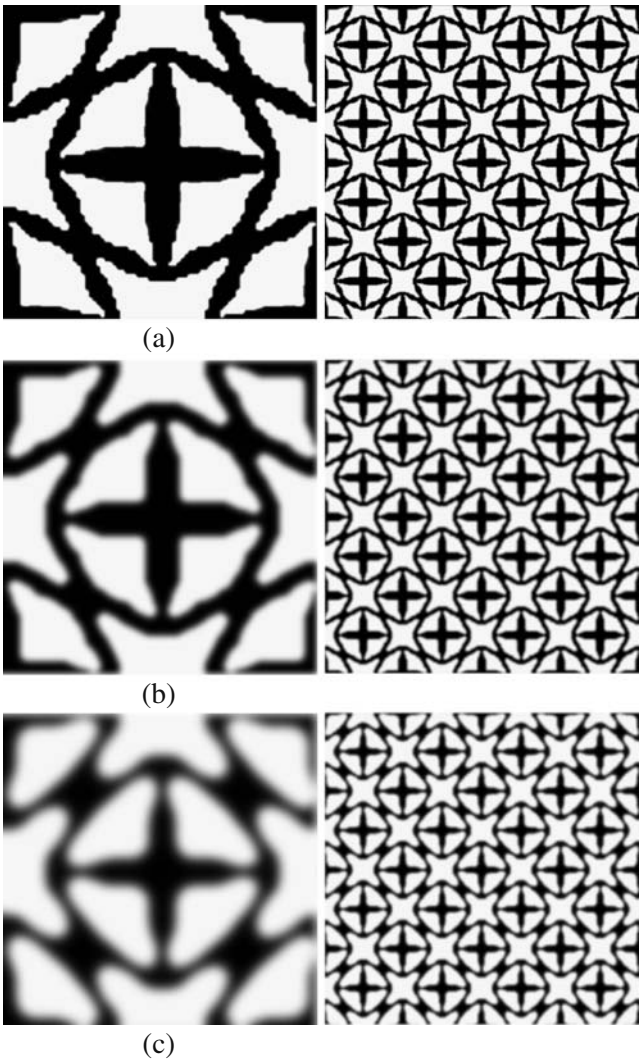

Fig. 21 Unit cell pseudo-density distribution and corresponding composite material matrix for a material intended to have negative Poisson's ratio: **a** $r_{min} = 1$, $\Theta = 40.2\%$; **b** $r_{min} = 2$, $\Theta = 32.0\%$; **c** $r_{min} = 4$, $\Theta = 18.9\%$

8.3.4 Example 4—negative Poisson's ratio

The second example considers the design of a material with negative Poisson's ratio. In this case, the prescribed properties are

$$\mathbf{D} = \begin{bmatrix} 1.0 & -1.0 & 0 \\ -1.0 & 1.0 & 0 \\ 0 & 0 & 0.0 \end{bmatrix}. \quad (51)$$

The same property values for basic materials (+) and (−) and the same unit cell design domain, like in the previous example, are adopted. Unit cell designs for r_{min} equal to 1 (no gradation), 2, 4; 6, 10, and 20 are shown in Figs. 21 and 22. The corresponding obtained property values are described below:

$$\mathbf{D}^H\left(_{r_{min}=1}\right) = \begin{bmatrix} 1.1366 & -0.6732 & 0 \\ -0.6732 & 1.1366 & 0 \\ 0 & 0 & 0.0577 \end{bmatrix}$$

$$\mathbf{D}^H\left(_{r_{min}=2}\right) = \begin{bmatrix} 1.1180 & -0.5445 & 0 \\ -0.5445 & 1.1180 & 0 \\ 0 & 0 & 0.0757 \end{bmatrix}$$

$$\mathbf{D}^H\left(_{r_{min}=4}\right) = \begin{bmatrix} 0.9571 & -0.2464 & 0 \\ -0.2464 & 0.9571 & 0 \\ 0 & 0 & 0.1136 \end{bmatrix}$$

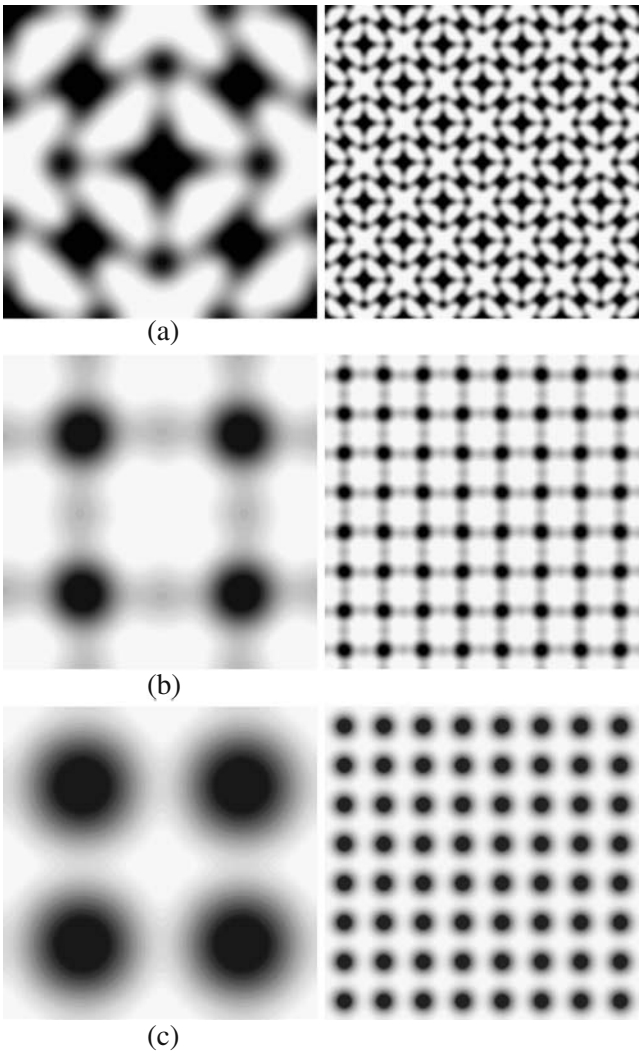

Fig. 22 Unit cell pseudo-density distribution and corresponding composite material matrix for a material intended to have negative Poisson's ratio: **a** $r_{min} = 6, \Theta = 8.8\%$; **b** $r_{min} = 10, \Theta = 4.3\%$; **c** $r_{min} = 20, \Theta = 10.3\%$

$$\mathbf{D}^H\left(_{r_{min}=6}\right) = \begin{bmatrix} 0.7399 & -0.0408 & 0 \\ -0.0408 & 0.7399 & 0 \\ 0 & 0 & 0.1141 \end{bmatrix}$$

$$\mathbf{D}^H\left(_{r_{min}=10}\right) = \begin{bmatrix} 0.4792 & 0.0363 & 0 \\ 0.0363 & 0.4792 & 0 \\ 0 & 0 & 0.0553 \end{bmatrix}$$

$$\mathbf{D}^H\left(_{r_{min}=20}\right) = \begin{bmatrix} 0.2830 & 0.0467 & 0 \\ 0.0467 & 0.2830 & 0 \\ 0 & 0 & 0.0624 \end{bmatrix}. \quad (52)$$

For the 0–1 problem a Poisson's ratio close to -1 could not be obtained. The reason is that the method did not allow for flexible hinges, thus, the lower value for the Poisson's ratio that could be obtained was -0.6732 . The plot of the Poisson's ratio value as a function of r_{min} (gradient length) is shown in Fig. 23. Like in the previous example, it is noticed that the Poisson's ratio value does not change significantly after r_{min} =10. The difference between each of the above cases and the reference property of (51) in the max norm is 32.7%, 45.6%, 75.4%, 95.9%, 103.6%, 104.7%, respectively. As in the previous section, one observes that the solution degrades when imposing gradient control. Moreover, at the end (largerr_{min}), the Poisson's ratio is not negative.

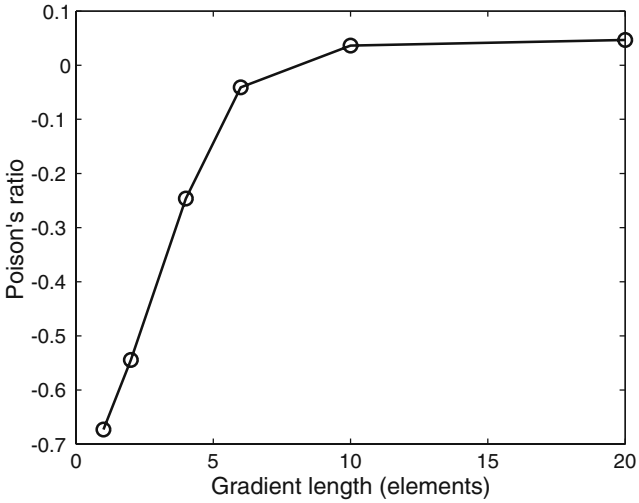

Fig. 23 Poisson's ratio as a function of r_{min} (gradient length)

9 Conclusions

This work shows that the material design method based on the continuum topology optimization together with a gradient control technique is applicable to the design of FGM microstructures. The continuous material distribution leads to a natural representation of the change of material properties inside the design domain in a continuous fashion, which is closely related to the FGM concept. The gradient control introduces a length scale in the process, which allows local control of the FGM gradation, and thus leads to feasible results. As expected, in the case of extreme materials, the presence of gradation moves the property values far from the extreme material property values. After a certain gradation control magnitude, the material behavior does not seem to be affected significantly.

The present work offers room for further extensions such as exploring graded three-dimensional architectures. Moreover, as indicated in the introduction, the present simulation framework can be used in conjunction with manufacturing techniques to achieve composites with locally graded microstructures. We notice that the resulting architecture has an additional

length scale associated with the material gradation. This poses a challenge for material processing, but also offers opportunities for developing new material microstructures with tailored functionality. In addition, the material design methodology adopted here can be used by material engineers who want to explore different microstructural architectures, including locally graded material systems. In fact, the development of novel techniques such as spark plasma sintering, co-extrusion, selective laser melting, and solid free-form fabrication, e.g. 3D printing, may allow the fabrication of graded microstructures (e.g. printwise and layerwise) in conjunction with a computer model such as the one presented in this work.

Acknowledgements We acknowledge the USA NSF through the project *CMS*#0303492 "Inter-Americas Collaboration in Materials Research and Education" (PI, Prof. W. Soboyejo, Princeton University). The first author acknowledges FAPESP — "Fundação de Amparo à Pesquisa do Estado de São Paulo" (Research Foundation of São Paulo State, Brazil), for providing him the Visiting Scientist award at the University of São Paulo (USP) through project number 2008/51070-0. The second author also thanks FAPESP and CNPq – "Conselho Nacional de Desenvolvimento Científico e Tecnológico" (National Council for Scientifical and Technological Development), both from Brazil, for financial support. The third author acknowledges the fellowship provided by Vietnam Education Foundation (VEF). Finally, we are grateful to Prof. Svanberg for providing the source code for the method of Moving Asymptotes (MMA).

Appendix A: H-S upper and lower limits

For isotropic materials, the upper and lower limits of H-S are given as a function of the bulk modulus (K) and shear modulus (G). Thus, considering two isotropic materials indicated by superscripts (+) and (−), whose properties follow the relation $K^+ > K^-$ and $G^+ > G^-$, the upper and lower limits for the bulk modulus, K_{max} and K_{min}, respectively, are given by (Hashin and Shtrikman 1963; Bendsøe and Sigmund 2003):

$$K_{max} = (1-\rho)\,K^- + \rho K^+ - \frac{(1-\rho)\,\rho\left(K^+ - K^-\right)^2}{(1-\rho)\,K^+ + \rho K^- + G^+} \tag{53}$$

$$K_{\min} = (1-\rho)\,K^- + \rho K^+ - \frac{(1-\rho)\,\rho\left(K^+ - K^-\right)^2}{(1-\rho)\,K^+ + \rho K^- + G^-}, \tag{54}$$

and the upper and lower limits, G_{max} and G_{min}, respectively, are given by:

$$G_{\max} = (1-\rho)\,G^- + \rho G^+ - \frac{(1-\rho)\,\rho\left(G^+ - G^-\right)^2}{(1-\rho)\,G^+ + \rho G^- + \frac{K^+ G^+}{K^+ + 2\,G^+}} \tag{55}$$

$$G_{\min} = (1-\rho)\,G^- + \rho G^+ - \frac{(1-\rho)\,\rho\left(G^+ - G^-\right)^2}{(1-\rho)\,G^+ + \rho G^- + \frac{K^- G^-}{K^- + 2G^-}}. \tag{56}$$

Appendix B: Sensitivity of material model based on H-S bounds

The derivative $\partial \mathbf{D}^m/\partial\rho$ can be obtained through the expression

$$\frac{\partial \mathbf{D}^m}{\partial \rho} = \frac{\partial \mathbf{D}^m}{\partial E^m}\left(\frac{\partial E^m}{\partial K^m}\frac{\partial K^m}{\partial \rho} + \frac{\partial E^m}{\partial G^m}\frac{\partial G^m}{\partial \rho}\right) + \frac{\partial \mathbf{D}^m}{\partial \nu^m}\left(\frac{\partial \nu^m}{\partial K^m}\frac{\partial K^m}{\partial \rho} + \frac{\partial \nu^m}{\partial G^m}\frac{\partial G^m}{\partial \rho}\right). \tag{57}$$

By differentiating (16), we obtain

$$\frac{\partial E^m}{\partial K^m} = \frac{9}{\left(1 + 3\frac{K^m}{G^m}\right)} - \frac{27K^m}{G^m\left(1 + 3\frac{K^m}{G^m}\right)^2} \tag{58}$$

$$\frac{\partial E^m}{\partial G^m} = \frac{27\,(K^m)^2}{\left[\left(1 + 3\frac{K^m}{G^m}\right)G^m\right]^2}, \tag{59}$$

and

$$\frac{\partial \nu^m}{\partial K^m} = \frac{(2/3)\,G^m}{(K^m)^2\left(2 + (2/3)\,\frac{G^m}{K^m}\right)} + \frac{(2/3)\left(1 - (2/3)\,\frac{G^m}{K^m}\right)G^m}{\left[\left(2 + (2/3)\,\frac{G^m}{K^m}\right)K^m\right]^2} \tag{60}$$

$$\frac{\partial \nu^m}{\partial G^m} = -\frac{2/3}{K^m\left(2 + (2/3)\,\frac{G^m}{K^m}\right)} - \frac{2/3\left(1 - (2/3)\,\frac{G^m}{K^m}\right)}{\left(2 + (2/3)\,\frac{G^m}{K^m}\right)^2 K^m}. \tag{61}$$

The derivatives $\partial K^m/\partial\rho$ and $\partial G^m/\partial\rho$ can be obtained by differentiating (14) and (15):

$$\frac{\partial K^m}{\partial \rho} = \kappa\frac{\partial K_{\max}(\rho)}{\partial \rho} + (1-\kappa)\frac{\partial K_{\min}(\rho)}{\partial \rho} \tag{62}$$

$$\frac{\partial G^m}{\partial \rho} = \kappa\frac{\partial G_{\max}(\rho)}{\partial \rho} + (1-\kappa)\frac{\partial G_{\min}(\rho)}{\partial \rho}. \tag{63}$$

Finally, considering $K_{\max}(\rho)$, $K_{\min}(\rho)$, $G_{\max}(\rho)$, and $G_{\min}(\rho)$ given by (53), (54), (55), and (56), we obtain

$$\frac{\partial K_{\max}}{\partial \rho} = -K^- + K^+ + \frac{\rho\left(K^+ - K^-\right)^2}{(1-\rho)\,K^+ + \rho K^- + G^+} - \frac{(1-\rho)\left(K^+ - K^-\right)^2}{(1-\rho)\,K^+ + \rho K^- + G^+} + \frac{(1-\rho)\,\rho\left(K^+ - K^-\right)^2\left(K^- - K^+\right)}{\left((1-\rho)\,K^+ + \rho K^- + G^+\right)^2} \tag{64}$$

$$\frac{\partial K_{\min}}{\partial \rho} = -K^- + K^+ + \frac{\rho\left(K^+ - K^-\right)^2}{(1-\rho)\,K^+ + \rho K^- + G^-} - \frac{(1-\rho)\left(K^+ - K^-\right)^2}{(1-\rho)\,K^+ + \rho K^- + G^-} + \frac{(1-\rho)\,\rho\left(K^+ - K^-\right)^2\left(K^- - K^+\right)}{\left((1-\rho)\,K^+ + \rho K^- + G^-\right)^2} \tag{65}$$

$$\frac{\partial G_{\max}}{\partial \rho} = -G^- + G^+ + \frac{\rho\left(G^+ - G^-\right)^2}{(1-\rho)\,G^+ + \rho G^- + \frac{K^+G^+}{K^+ + 2G^+}} - \frac{(1-\rho)\left(G^+ - G^-\right)^2}{(1-\rho)\,G^+ + \rho G^- + \frac{K^+G^+}{K^+ + 2G^+}} + \frac{(1-\rho)\,\rho\left(G^+ - G^-\right)^2\left(G^- - G^+\right)}{\left((1-\rho)\,G^+ + \rho G^- + \frac{K^+G^+}{K^+ + 2G^+}\right)^2} \tag{66}$$

$$\frac{\partial G_{\min}}{\partial \rho} = -G^- + G^+ + \frac{\rho\left(G^+ - G^-\right)^2}{(1-\rho)\,G^+ + \rho G^- + \frac{K^-G^-}{K^- + 2G^-}} - \frac{(1-\rho)\left(G^+ - G^-\right)^2}{(1-\rho)\,G^+ + \rho G^- + \frac{K^-G^-}{K^- + 2G^-}} + \frac{(1-\rho)\,\rho\left(G^+ - G^-\right)^2\left(G^- - G^+\right)}{\left((1-\rho)\,G^+ + \rho G^- + \frac{K^-G^-}{K^- + 2G^-}\right)^2}. \tag{67}$$

Thus, the sensitivity for the material model based on the H-S bounds can be obtained.

References

Allaire G (2002) Shape optimization by the homogenization method. Applied mathematical sciences, vol 146. ISBN-10: 0387952985. Springer, New York

Bendsøe MP, Kikuchi N (1988) Generating optimal topologies in structural design using a homogenization method. Comput Methods Appl Mech Eng 71(2):197–224

Bendsøe MP, Sigmund O (2003) Topology optimization: theory, methods and application. Springer, Berlin

Bruyneel M, Duysinx P, Fleury C (2002) A family of MMA approximations for structural optimization. Struct Multidisc Optim 24(4):263–276

Carbonari RC, Silva ECN, Paulino GH (2007) Topology optimization design of functionally graded bimorph-type piezoelectric actuators. Smart Mater Struct 16(6):2605–2620

Chen BC, Silva ECN, Kikuchi N (2001) Advances in computational design and optimization with application to MEMS. Int J Numer Methods Eng 52(1–2):23–62

Cherkaev A (2000) Variational methods for structural optimization. Applied mathematical sciences, vol 140. ISBN-10: 0387984623. Springer, New York

Cherkaev A, Gibiansky LV (1993) Coupled estimates for the bulk and shear moduli of a 2-dimensional isotropic elastic composite. J Mech Phys Solids 41(5):937–980

Cherkaev A, Gibiansky LV (1996) Extremal structures of multiphase heat conducting composites. Int J Solids Struct 33(18):2609–2623

Cherkaev A, Kohn R (1997) Topics in the mathematical modelling of composite materials. ISBN-10: 3764336625. Birkhauser, Boston

Cox SJ, Dobson DC (1999) Maximizing band gaps in two-dimensional photonic crystals. SIAM J Appl Math 59(6):2108–2120

Cox SJ, Dobson DC (2000) Band structure optimization of two-dimensional photonic crystals in H-polarization. J Comput Phys 158(2):214–224

Crumm AT, Halloran JW (1998) Fabrication of microconfigured multicomponent ceramics. J Am Ceram Soc 81(4):1053–1057

Crumm AT, Halloran JW, Silva ECN, de Espinosa FM (2007) Microconfigured piezoelectric artificial materials for hydrophones. J Mater Sci 42(11):3944–3950

Diaz AR, Benard A (2003) Designing materials with prescribed elastic properties using polygonal cells. Int J Numer Methods Eng 57(3):301–314

Gibiansky LV, Sigmund O (2000) Multiphase composites with extremal bulk modulus. J Mech Phys Solids 48(3):461–498

Gibiansky LV, Torquato S (1995) Rigorous link between the conductivity and elastic-moduli of fiber-reinforced composite-materials. Philos Trans R Soc Lond Ser A Math Phys Sci 353(1702):243–278

Gibiansky LV, Torquato S (1999) Matrix laminate composites: realizable approximations for the effective moduli of piezoelectric dispersions. J Mater Res 14(1):49–63

Guedes JM, Kikuchi N (1990) Preprocessing and postprocessing for materials based on the homogenization method with adaptive finite-element methods. Comput Methods Appl Mech Eng 83(2):143–198

Guedes JM, Rodrigues HC, Bendsøe MP (2003) A material optimization model to approximate energy bounds for cellular materials under multiload conditions. Struct Multidisc Optim 25(5–6):446–452

Guest JK, Prévost JH, Belytschko T (2004) Achieving minimum length scale in topology optimization using nodal design variables and projection functions. Int J Numer Methods Eng 61:238–254

Hashin Z, Shtrikman S (1963) A variational approach of the theory of elastic behavior of multiphase materials. J Mech Phys Solids 11:127–140

Kim JH, Paulino GH (2002) Isoparametric graded finite elements for nonhomogeneous isotropic and orthotropic materials. ASME J Appl Mech 69(4):502–514

Kohn RV, Strang G (1986a) Optimal design and relaxation of variational problems, part I. Commun Pure Appl Math 39(1):113–137

Kohn RV, Strang G (1986b) Optimal design and relaxation of variational problems, part II. Commun Pure Appl Math 39(2):139–182

Kohn RV, Strang G (1986c) Optimal design and relaxation of variational problems, part III. Commun Pure Appl Math 39(3):353–377

Larsen UD, Sigmund O, Bouwstra S (1997) Design and fabrication of compliant micromechanisms and structures with negative Poisson's ratio. J Microelectromechanical Syst 6(2): 99–106

Lipton R, Northrup J (1994) Optimal bounds on the inplane shear moduli for orthotropic elastic composites. SIAM J Appl Math 54(2):428–442

Matsui K, Terada K (2004) Continuous approximation of material distribution for topology optimization. Int J Numer Methods Eng 59:1925–1944

Mazumder J, Schifferer A, Choi J (1999) Direct materials deposition: designed macro and microstructure. Mater Res Innov 3(3):118–131

Mazumder J, Dutta D, Kikuchi N, Ghosh A (2000) Closed loop direct metal deposition: art to part. Opt Lasers Eng 34 (4–6):397–414

Milton GW, Cherkaev AV (1995) Which elasticity tensors are realizable? J Eng Mater Technol Trans ASME 117(4): 483–493

Miyamoto Y, Kaysser WA, Rabin BH, Kawasaki A, Ford RG (1999) Functionally graded materials: design, processing and applications. Kluwer Academic, Dordrecht

Murat F, Tartar L (1985) Optimality conditions and homogenization. In: Mario A, Modica L, Spagnolo S (eds) Nonlinear variational problems. Pitman, Boston, pp 1–8

Neves MM, Rodrigues H, Guedes JM (2000) Optimal design of periodic linear elastic microstructures. Comput Struct 76 (1–3):421–429

Neves MM, Sigmund O, Bendsøe MP (2002) Topology optimization of periodic microstructures with a penalization of highly localized buckling modes. Int J Numer Methods Eng 54(6):809–834

Paulino GH, Jin Z-H, Dodds Jr RH (2003) Failure of functionally graded materials. In: Karihaloo B, Knauss WG (eds) Comprehensive structural integrity, vol 2, chapter 13. Elsevier Science, Oxford, pp 607–644

Paulino GH, Silva ECN (2005) Design of functionally graded structures using topology optimization. Mat Sci Forum 492–493:435–440

Pindera M-J, Aboudi J, Arnold SM (1995) Limitations of the uncoupled, RVE-based micromechanical approach in the analysis of functionally graded composites. Mech Mater 20(1):77–94

Qi H, Kikuchi N, Mazumder J (2004) Interface study and boundary smoothing on designed composite material microstructures for manufacturing purposes. Struct Multidisc Optim 26(5):326–332

Qi J, Halloran JW (2004) Negative thermal expansion artificial material from iron-nickel alloys by oxide co-extrusion with reductive sintering. J Mater Sci 39(13):4113–4118

Rahmatalla S, Swan CC (2003) Form finding of sparse structures with continuum topology optimization. ASCE J Struct Eng 129(12):1707–1716

Rahmatalla SF, Swan CC (2004) A Q4/Q4 continuum topology optimization implementation. Struct Multidisc Optim 27:130–135

Reiter T, Dvorak GJ, Tvergaard V (1997) Micromechanical models for graded composite materials. J Mech Phys Solids 45(8):1281–1302

Sanchez-Palencia E (1980) Non-homogeneous media and vibration theory. Lectures notes in physics 127. Springer, Berlin

Sigmund O (1994) Materials with prescribed constitutive parameters—an inverse homogenization problem. Int J Solids Struct 31(17):2313–2329

Sigmund O (1995) Tailoring materials with prescribed elastic properties. Mech Mater 20(4):351–368

Sigmund O (2000) A new class of extremal composites. J Mech Phys Solids 48(2):397–428

Sigmund O, Jensen JS (2003) Systematic design of phononic band-gap materials and structures by topology optimization. Philos Trans R Soc Lond Ser A Math Phys Sci 361(1806):1001–1019

Sigmund O, Torquato S (1996) Composites with extremal thermal expansion coefficients. Appl Phys Lett 69(21): 3203–3205

Sigmund O, Torquato S (1997) Design of materials with extreme thermal expansion using a three-phase topology optimization method. J Mech Phys Solids 45(6):1037–1067

Sigmund O, Torquato S (1999) Design of smart composite materials using topology optimization. Smart Mater Struc 8(3):365–379

Sigmund O, Torquato S, Aksay IA (1998) On the design of 1–3 piezocomposites using topology optimization. J Mater Res 13(4):1038–1048

Silva ECN, Fonseca JSO, Kikuchi N (1998) Optimal design of periodic piezocomposites. Comput Methods Appl Mech Eng 159(1–2):49–77

Silva ECN, Fonseca JSO, de Espinosa FM, Crumm AT, Brady GA, Halloran JW, Kikuchi N (1999a) Design of piezocomposite materials and piezoelectric transducers using topology optimization - Part I. Arch Comput Methods Eng 6(2): 117–182

Silva ECN, Nishiwaki S, Fonseca JSO, Kikuchi N (1999b) Optimization methods applied to material and flextensional actuator design using the homogenization method. Comput Methods Appl Mech Eng 172(1–4): 241–271

Silva ECN, Paulino GH (2004) Topology optimization applied to the design of functionally graded material (FGM) structures. In: Proceedings of 21st international congress of theoretical and applied mechanics (ICTAM) 2004, 15–21 August 2004, Warsaw

Smith WA (1992) Limits to the enhancement of piezoelectric transducers achievable by materials engineering. Proc IEEE Ultrason Symp 1:697–702

Suresh S, Mortensen A (1988) Fundamentals of functionally graded materials. IOM Communications, London

Svanberg K (1987) The method of moving asymptotes—a new method for structural optimization. Int J Numer Methods Eng 24:359–373

Torquato S (2002) Random heterogeneous materials—microstructure and macroscopic properties. ISBN-10: 0387951679. Springer, New York

Torquato S, Hyun S, Donev A (2003) Optimal design of manufacturable three-dimensional composites with multifunctional characteristics. J Appl Phys 94(9):5748–5755

Van Hoy C, Barda A, Griffith M, Halloran JW (1998) Microfabrication of ceramics by co-extrusion. J Am Ceram Soc 81(1):152–158

Yin HM, Sun LZ, Paulino GH (2004) Micromechanics-based elastic model for functionally graded materials with particle interactions. Acta Mater 52(12):3535–3543